Geochemistry Geophysics Geosystems G3

Article
Volume 12, Number 3
23 March 2011
Q0A008, doi:10.1029/2010GC003335
ISSN: 1525-2027

Published by AGU and the Geochemical Society

Spatial and temporal evolution of the megasplay fault in the Nankai Trough

Gaku Kimura
Department of Earth and Planetary Science, Graduate School of Science, University of Tokyo, 7-3-1 Hongo, Bunkyo-ku, Tokyo 113-0033, Japan (gaku@eps.s.u-tokyo.ac.jp)

Gregory F. Moore
Department of Geology and Geophysics, University of Hawaii at Mānoa, 1680 East-West Road, Post 813, Honolulu, Hawaii 96822, USA (gmoore@hawaii.edu)

Michael Strasser
Research Center Ocean Margins, University of Bremen, Leobenerstrasse, MARUM Building, Room 1220, D-28359 Bremen, Germany (mstrasser@uni-bremen.de)

Elizabeth Screaton
Department of Geological Science, University of Florida, 241 Williamson Hall, PO Box 112120, Gainesville, Florida 32611, USA (screaton@ufl.edu)

Daniel Curewitz
Heroy Geology Laboratory, Syracuse University, Syracuse, New York 13244-1070, USA (dcurewit@syr.edu)

Carolyn Streiff and Harold Tobin
Department of Geoscience, University of Wisconsin-Madison, 1215 W. Dayton Street, Madison, Wisconsin 53706, USA (streiff@wisc.edu; htobin@.wisc.edu)

[1] The temporal and spatial evolution of a seismogenic megasplay fault in the Kumano area, Nankai Trough (southwest Japan), is revealed by detailed investigation of the three-dimensional structure of the shallow portions of the fault, combined with the results of drilling and dating of cores from Integrated Ocean Drilling Program (IODP) Expedition 316. The ENE striking eastern portion of the splay fault has remained active since the inception of faulting at ~1.95 Ma. The recent shortening rate is ~1 m/kyr, which represents ~1.5%–2.5% of the total plate convergence rate of ~40–65 m/kyr. The NE striking western portion of the splay fault exhibits a different mode of activity. Early stage activity (before 1.55 Ma) was similar to the eastern portion, but the fault was inactive between 1.55 and 1.24 Ma. The fault was reactivated for a short time at ~1.24 Ma but again ceased activity after formation of the secondary branch and has been inactive since 1.24 Ma. Cessation of splay fault activity in the western domain after 1.55 Ma may be due to collision with a seamount and resulting bending of the accretionary prism in the splay fault footwall. Continuous activity of the eastern domain of the splay fault after 1.24 Ma may be related to geometrical favorability due to reorientation of the fault after the seamount passed beneath the imbricate thrust zone, leading to initiation of slightly oblique subduction.

Components: 11,900 words, 13 figures.

Keywords: splay fault; Nankai Trough; earthquake; tsunami; accrerionary prism; IODP.

Index Terms: 8170 Tectonophysics: Subduction zone processes (1031, 3060, 3613, 8413); 8010 Structural Geology: Fractures and faults; 7240 Seismology: Subduction zones (1207, 1219, 1240).

Received 23 August 2010; **Revised** 21 January 2011; **Accepted** 28 January 2011; **Published** 23 March 2011.

Kimura, G., G. F. Moore, M. Strasser, E. Screaton, D. Curewitz, C. Streiff, and H. Tobin (2011), Spatial and temporal evolution of the megasplay fault in the Nankai Trough, *Geochem. Geophys. Geosyst.*, *12*, Q0A008, doi:10.1029/2010GC003335.

Theme: Mechanics, Deformation, and Hydrologic Processes at Subduction Complexes, With Emphasis on the Nankai Trough Seismogenic Zone Experiment (NanTroSEIZE) Drilling Transect
Guest Editors: D. Saffer, P. Henry, and H. Tobin

1. Introduction

[2] Great earthquakes and tsunamis along subduction zones are generated when large areas of the plate boundary megathrust rupture, and slip along faults rapidly propagates close to the ocean floor. Tsunamis can be also generated when catastrophic submarine landslides are produced due to unstable slope collapse (e.g., New Guinea) [*Matsumoto and Tappin*, 2003]. Many studies have inferred that coseismic slip along splay faults that branch from the plate boundary megathrust may provide a mechanism by which earthquakes generate tsunamis [*Fukao*, 1979; *Plafker*, 1972; *Baba et al.*, 2006; *Tanioka and Satake*, 2001]. Therefore, understanding the 3-D geometry, quantifying the physical properties and stress conditions, and documenting the history of splay faults are all essential toward assessing their role in the plate boundary and coseismic slip.

[3] The character of the ocean floor and the geologic structure of splay faults at shallow depths provide important information about their geometry, mechanics, and tsunamigenic processes. Detailed geomorphological and geological investigations are, however, difficult because of the deep submarine occurrence of the faults. In addition, characteristics of subseafloor faults are expected to differ from well-studied active faults on land because the seabed is primarily within depositional regimes while on-land active fault exposures are commonly situated in erosive regimes. On-land fault exposures are easily eroded by water, whereas submarine fault scarps are situated under slow ocean bottom currents and rather stable conditions, even where exposed on the seabed. Such seabed exposures yield an advantage for investigation of recent tectonic activities. Active sediment deposition on the seafloor is especially significant because dating of fault activities is possible from the sedimentary record. Thus fine-scale observation of both the seabed and the internal geologic structure can provide a key to understanding the recent activity of subseafloor splay faults.

[4] At the Nankai Trough, where the Philippine Sea plate is subducting below southwest Japan at a rate of 4–6.5 cm/yr at an azimuth of ~300°–315° [*Seno et al.*, 1993; *Miyazaki and Heki*, 2001; *Zang et al.*, 2002], destructive earthquakes and tsunamis repeatedly occur [*Ando*, 1975]. Reflection seismic images have identified a splay fault as a first-order margin-dominating structure that extends more than 120 km along strike [*Park et al.*, 2002b; *Moore et al.*, 2007, 2009; *Kimura et al.*, 2007; *Bangs et al.*, 2009]. Mechanical arguments [*Wang and Hu*, 2006; *Kame et al.*, 2003], seismic and tsunami waveform inversions [*Kikuchi et al.*, 2003; *Baba et al.*, 2006; *Tanioka and Satake*, 2001], and seismic reflection data strongly suggest that this fault, termed the "megasplay" by *Tobin and Kinoshita* [2006], is one of the primary coseismic faults that may have contributed to generating devastating historic earthquakes and tsunamis. In the Kumano Basin area, the megasplay fault branches from the plate boundary thrust ~50 km landward of the trench (Figures 1b and 2).

[5] Stage 1 of the Integrated Ocean Drilling Program's (IODP) Nankai Trough Seismogenic Zone Experiment (NantroSEIZE) was conducted from September 2007 to February 2008 and successfully acquired geological and physical properties data, including age dating of cores from the shallow

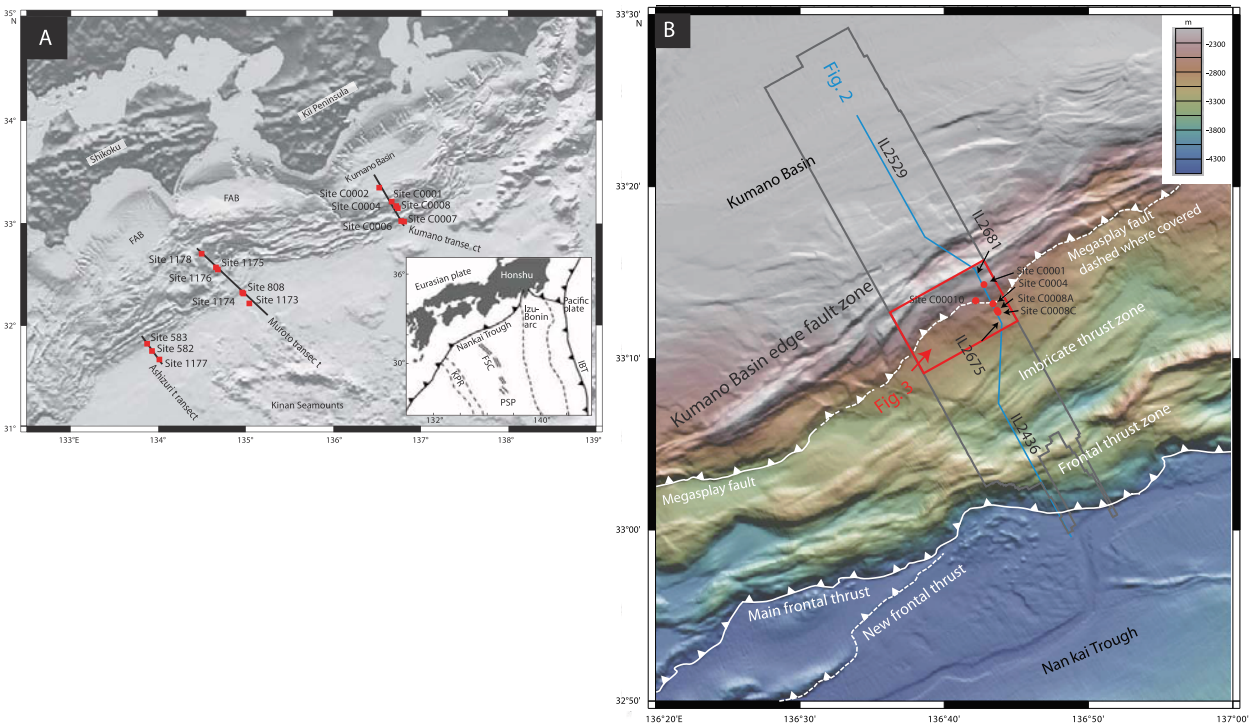

Figure 1. (a) Regional bathymetry of northern Shikoku Basin and Nankai Trough region showing previous DSDP/ODP and current IODP drilling transects. FAB, forearc basin. Inset is tectonic map showing plate tectonic setting of the region. IBT, Izu-Bonin Trench; KPR, Kyushu-Palau Ridge; FSC, fossil spreading center; PSP, Philippine Sea plate. (b) Multibeam bathymetry of the Kumano Basin region. Solid line indicates 3-D seismic survey; circles indicate NanTroSEIZE Stage 1 drill sites. Details of bathymetry data acquisition and processing are summarized by *Ike et al.* [2008]. Figures are modified from *Moore et al.* [2009].

portion of the megasplay fault [*Kimura et al.*, 2008; *Kinoshita et al.*, 2009]. Substantial long-term slip of the splay fault is documented by sequence boundaries and progressive landward tilting of strata in the fore-arc basin and by drilling into the shallow portion of the splay fault [*Kinoshita et al.*, 2009; *Strasser et al.*, 2009]. Prior to drilling (April-May 2006), a joint Japanese-U.S. group contracted a commercial 3-D seismic survey to enhance our understanding of the structural and stratigraphic

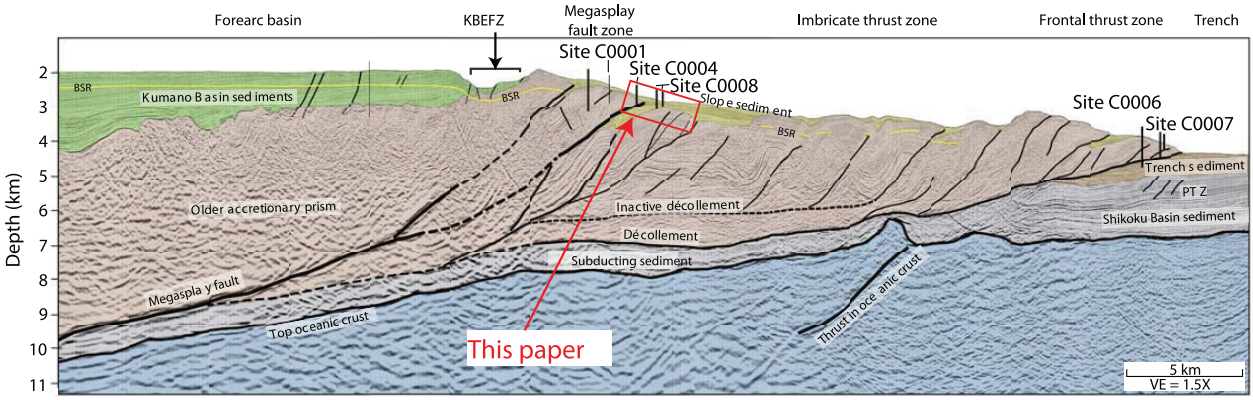

Figure 2. Interpretation of composite seismic line [*Moore et al.*, 2009] extracted from 3-D seismic volume. The line crosses through (or near) all NantroSEIZE Stage 1 drill sites (location shown in Figure 1b).Only a few representative faults are shown. Dashed lines indicate less certain fault locations. Morphotectonic zones are shown between the two sections. KBEFZ, Kumano Basin edge fault zone; PTZ, protothrust zone; BSR, bottom-simulating reflector; VE, vertical exaggeration.

setting of the proposed drill sites (see *Moore et al.* [2009] for details). Petroleum Geoservices (PGS) acquired a 12 × 56 km 3-D data volume using two arrays of 28 Sodera G-guns, each totaling 3090 in^3 (51 L) fired alternately at 37.5 m intervals, with seismic signals received by four 4500 m long hydrophone cables, each with 360 receiver groups at 12.5 m spacing. Data processing included 3-D prestack depth migration (PSDM) that provides sharp images of the shallow part of the accretionary prism, allowing us to map details of the splay fault structure and associated sediment deformation throughout the region.

[6] In this paper, we present the 3-D history and recent activities of the splay fault based on the combination of detailed analysis of 3-D seismic data from the shallow parts of the splay fault, seabed topography, and geological and structural data from core and boreholes. We further discuss factors that control the fault activity at shallow depths that are intimately linked with coseismic tsunami generation along this margin.

2. Regional Setting of the Kumano Transect in the Nankai Trough

[7] The Nankai Trough, as the type example of a subduction zone accreting a thick terrigenous sediment section, has been a site of intense study, including Deep Sea Drilling Project (DSDP) and Ocean Drilling Program (ODP) drilling [*Karig et al.*, 1975; *Taira et al.*, 1991; *Moore et al.*, 2001], numerous two-dimensional (2-D) and three-dimensional (3-D) seismic reflection surveys and ocean bottom seismometer wide-angle seismic surveys [e.g., *Aoki et al.*, 1982; *Moore et al.*, 1990; *Park et al.*, 2002a, 2002b; *Kodaira et al.*, 2006; *Nakanishi et al.*, 2008], and heat flow and submersible surveys [e.g., *Ashi et al.*, 2002]. The NanTroSEIZE project is an ongoing multidisciplinary scientific investigation of seismogenic processes in the Nankai Trough, focused on the Kumano Transect south of the Kii Peninsula, Honshu, Japan (Figure 1). The Kumano transect is within the region that ruptured during the 1944 and 1946 earthquakes [*Baba and Cummins*, 2005], and this portion of the seismogenic zone is the target of IODP drilling [*Tobin and Kinoshita*, 2006].

[8] Figures 1b and 2 illustrate the main regional morphotectonic zones in the Kumano Transect on the basis of a high-resolution multibeam bathymetric data set, 2-D seismic reflection studies, and the 3-D volume that includes NantroSEIZE Stage 1 drill sites [*Moore et al.*, 2009]. Outboard of the trench on this transect, (Figure 2), a ~1.3 km thick wedge of trench sediments overlies ~1.1 km of Shikoku Basin deposits, which consist of regional hemipelagic sediments, and the Philippine Sea plate igneous basement. All of the trench deposits and at least half of the Shikoku Basin deposits are accreted to form a wide accretionary prism in this region, with a frontal thrust zone at the toe of the prism and a landward imbricate thrust zone (ITZ) (Figures 1b and 2) [*Park et al.*, 2002b; *Moore et al.*, 2009]. Beneath the trench upper slope and Kumano Basin, the megasplay fault cuts across the older part of the accretionary prism. The megasplay fault can be traced from deep below the accretionary wedge at ~10 km, where it lies ~1 km above the top of the subducting crust (Figure 2). It cuts discontinuously up through the accretionary wedge along several branches [*Moore et al.*, 2007, 2009]. Deep segments of the splay fault are continuous along strike across the entire 12 km 3-D survey width, with shallower segments continuing typically 3–5 km along strike. Many segments along the splay fault system have reversed polarity reflections relative to the seafloor and high amplitudes relative to adjacent stratigraphic horizons [*Streiff et al.*, 2009].

[9] The Kumano fore-arc basin is bounded on the southeast by a topographic valley situated atop the break between the basin and the upper part of the trench slope (Figure 2). Beneath this valley is the Kumano Basin edge fault zone (KBEFZ) that may have a combination of normal and strike-slip faults [*Martin et al.*, 2010].

3. Topography and Stratigraphy Around the Shallow Tip of the Megasplay Fault

[10] In this section, we describe the high-resolution topography and stratigraphy obtained by IODP Expedition 316 drilling around the megasplay fault tip in the 3-D box.

3.1. Seabed Topography

[11] High-resolution seabed topography derived from the 3-D seismic data shows variations perpendicular to, and along strike of, the regional slope. Seaward of the KBEFZ, which is characterized by NE trending to ENE trending ridges shallower than 2000 m, stepwise slopes are clearly developed (Figure 3). At ~2100–2200 m, a gentle slope constituting an upper slope basin is almost parallel to the KBEFZ (Figure 3). The midslope,

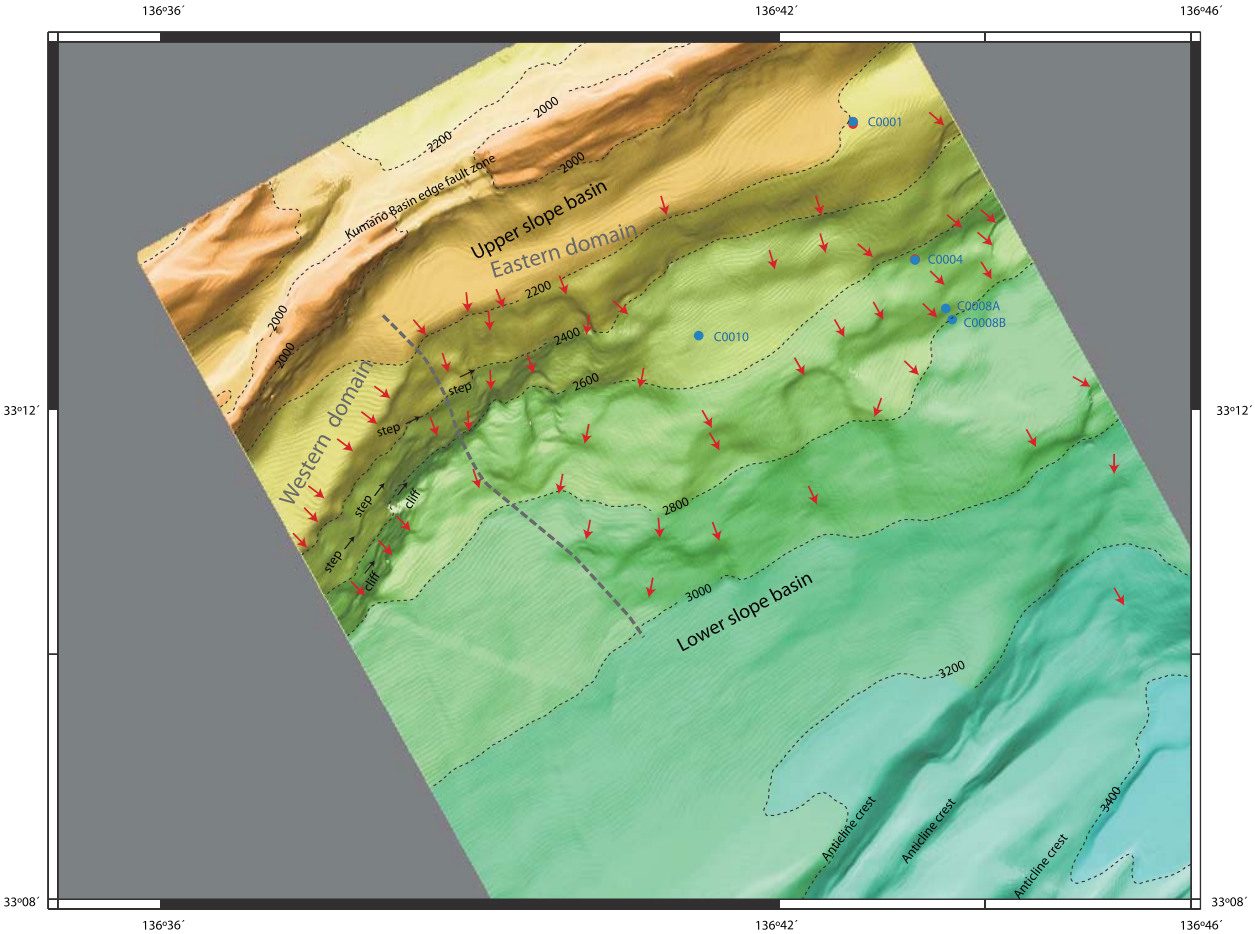

Figure 3. A high-resolution topographic map of survey area extracted from the 3-D seismic volume (error range is ±5 m). Blue circles show drill sites of IODP NantroSEIZE [*Kinoshita et al.*, 2009]. Red arrows represent slump scars of submarine landslides. The arrows also indicate sliding directions. Bathymetric contour lines are labeled in meters. Location of the area is shown in Figure 1b.

between ~2200 m and ~2500 m, is rather steep, with a dip of > 10°. The lower slope region, deeper than ~2500–2600 m, generally has gentle slopes, forming lower slope basins (Figure 3). The seabed deeper than ~3200 m (imbricate thrust zone in Figure 1b) exhibits ridge-basin topography typical of fold-and-thrust belts developed in many accretionary prisms [e.g., *Morley*, 2009].

[12] We define two regional domains (eastern and western) with a boundary at 136°38′–40′ (Figure 3) based on clear along-strike variations. The surface slope in the eastern domain is much gentler than that in the western domain. The slope of the eastern domain strikes ENE, whereas the western slope strikes NE. The gentle upper and lower slopes have dip angles of ~4°. The steep middle slope of the western region has a rough surface and is characterized by "slump scar" topography consisting of horseshoe-like shapes along the southeastern edge of the gentle upper slope (Figure 3). The down-slip direction of the slides on the western steep slope is to the southeast, perpendicular to the strike of the slope edge, and the slide masses appear to have been deposited around the foot of the steep slopes.

[13] The midslope of the eastern domain between ~2200 m and ~2400 m has a smooth surface, in contrast to that of the western slope. The lower slope of the eastern domain has two parts: one from ~2400 to ~3000 m that contains many U-shaped landslides and one deeper than ~3000 m that has a smooth surface. These features are also in contrast to the western domain, where the lower slope dips gradually SE and has a rather smooth surface from ~2600 m to ~3000 m (Figure 3).

3.2. Stratigraphy

[14] Four holes (C0001A, C0004A, C0008A and C0008C) were drilled in the eastern slope domain

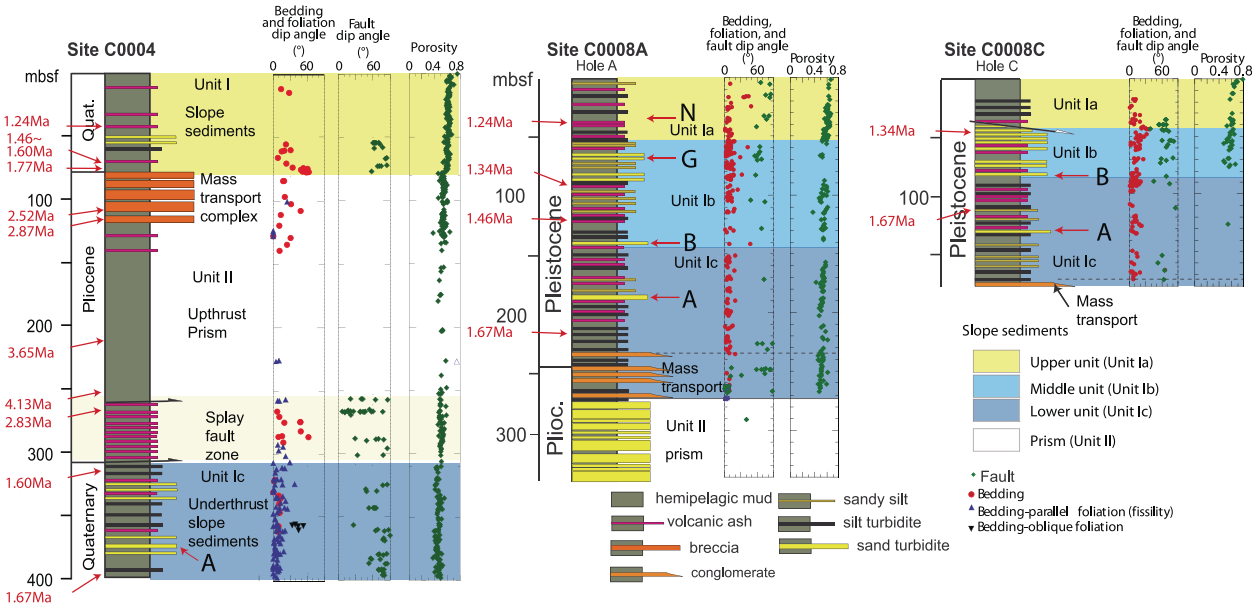

Figure 4. Geologic columns of core recovered from the sites C0004, C0008A, and C0008C by IODP Expedition 316 [*Kimura et al.*, 2008, *Kinoshita et al.*, 2009].

during IODP NantroSEIZE Stage 1 (Figures 1–4). Coring at Holes C0008A and C0008C provides a reference section for sediments in the lower slope basin (Figure 4), and Site C0004 sampled the accretionary prism and slope sediments lying both above the splay fault footwall and beneath the prism that has been upthrust along the splay fault. Figure 4 is a graphic column of lithology, age, structure, and porosity of the sediments [*Expedition 316 Scientists*, 2009a].

[15] *Expedition 316 Scientists* [2009a] classified sediments into two units, the slope sediments (Unit I) and underlying accretionary prism (Unit II) on the basis of lithology and setting. We refine the slope sediment classification into three units (Ia-Ic) on the basis of core description and key traceable horizons on the 3-D seismic profiles (Figure 4). Several geological phenomena, such as unconformities or mass transport complex (MTC), are generally critical for unit definition; however, many of these are local features that are difficult to trace over wide areas. Therefore, we used key horizons or marker beds (a turbidite or a tuff deposit in the drill cores, for example) to trace the section across the entire area of interest. We define the key horizons first on seismic profiles at Holes C0008A and C0008C. We name the horizons from A to N sequentially in ascending order and identified horizons A, B, G and N as traceable key beds in the region (Figure 4).

3.2.1. Unit I (Slope Sediments) at C0008A and C0008C

3.2.1.1. Unit Ia

[16] Topmost unit of slope sediments from horizon G to the seabed. Nannofossils and magnetostratigraphy document that the upper ~10 m thick sequence below the seabed is younger than 0.063 Ma. Unit Ia is composed mainly of silty mud and silty turbidites with several ash layers. Horizon N is a key bed, likely composed of ash that is traceable throughout the surveyed area. In Unit Ia, MTCs composed of mud clasts with mud matrix are recognized.

3.2.1.2. Unit Ib

[17] Slope sediments between horizon B and horizon G (Figure 4). Coarse turbidite and ash layers are abundant throughout the section, with interbedded silty mud and mud. Nannofossils and magnetostratigraphy show that Unit Ib ranges from 1.55 to 1.24 Ma in age (Figure 4) [*Expedition 316 Scientists*, 2009a; *Strasser et al.*, 2009]. Horizon B and horizon G produce distinctive reflections in the 3-D seismic data [*Expedition 316 Scientists*, 2009a] that are traceable throughout the entire investigated area. This unit may correlate to successions of interbedded sandy turbidites and mud layers. Nannofossil assemblages in Unit Ib show a mixed occurrence of young and old species, suggesting

reworking and possibly indicating upslope collapse as the sediment source [*Strasser et al.*, 2009].

3.2.1.3. Unit Ic

[18] Slope sediments beneath horizon B and above the unconformity on the prism, consisting of turbiditic sand (Figure 4). Cores at Sites C0008A and C0008C generally consist of greenish-gray silty clay with beds of sand, sandy silt, silt, and volcanic ash layers (Figure 4). At 234.55–272.46 m below seafloor (mbsf) in Hole C0008A and 170.9–176.20 mbsf in Hole C0008C, *Expedition 316 Scientists* [2009a] interpreted a latest Pliocene-lower Pleistocene sequence as a mass transport complex (MTC) that accumulated in the lower slope basin, possibly during an early stage of basin formation [*Strasser et al.*, 2009]. The unconformity between the underlying prism and the MTC occurs between 1.95 and 2.4 Ma based on nannofossil chronology and magnetostratigraphy [*Kinoshita et al.*, 2009; *Strasser et al.*, 2009]. The top of the mass transport complex ranges in age from 1.65 to 1.8 Ma (Figure 4). Horizon A is a key bed in the middle part of Unit Ic (Figure 4) and correlates to a coarse ~3.5 m thick sand.

[19] Dips of bedding planes of Units Ia–Ic in Holes C0008A and C0008C are dominantly to the south and are gentle in general but in places dip a few tens of degrees. Sediments at Hole C0008C are deformed primarily by normal faulting (Figure 4). A high concentration of normal faults is found between 35 and 80 mbsf near a discontinuity in bedding dip identified on seismic reflection profiles.

3.2.2. Unit I (Slope Sediments) at C0004

[20] Slope sediments at Site C0004 are separated into two units, one above the upthrust prism and another below the splay fault (Figure 4). Cover sediments above the prism are composed of gray silt, silty and sandy turbidites, and several ash layers. Their ages range from ~1.46–1.77 Ma to present (Figure 4). The total thickness of the slope sediments is 78.06 m at Site C0004, thinner than the comparable sequence at Hole C0008A. The age of the sediments overlaps with those at Holes C0008A and C0008C (Figure 5), but key horizons B, G and N are not recognized either in core or in seismic profiles. Therefore, unit subdivision and correlation with the subunits identified at Site C0008 is difficult. At the top of the prism section are 2.06–2.52 Ma mass transport deposits.

[21] Sediments underlying the splay fault consist of lower Pleistocene dark olive-gray silty clay with common thin sand and silt beds. These sediments can be correlated to the upper half of slope sediments in Unit Ic recovered at Site C0008A (Figures 3 and 4). The age of the sediments ranges from 1.67 to 1.60 Ma. The underthrust slope basin sediments exhibit horizontal to gently dipping bedding. Key horizon A composed of sand dominated layers is easily traced on the seismic profile to Hole C0008A.

3.2.3. Unit II: Accretionary Prism

[22] At Site C0004, the accretionary prism thrust over the Unit Ic slope sediment is composed dominantly of Pliocene hemipelagic mud with intercalated ash layers, several of which are prominent in the lower part of the splay fault zone (Figure 4) [*Expedition 316 Scientists*, 2009b]. Core recovery of the accretionary prism at Site C0004 was very poor but the result of logging while drilling during Expedition 314 [*Expedition 314 Scientists*, 2009] suggests a mudstone-dominated lithology. Lithology and age constraints suggest that these sediments are lower Shikoku Basin deposits recognized widely in the Shikoku Basin of the Philippine Sea plate [*Ike et al.*, 2008].

[23] Seismic reflection profile IL2675 (Figures 5 and 6) indicates that the projected depth of the splay fault at Site C0004 is around 290 mbsf. Structural observations of cores document an ~60 m thick fractured and brecciated zone between 256 and 315 mbsf. The occurrence of breccia with polished and slickensided surfaces below 256 mbsf marks the upper boundary of the fault zone. A documented (nannofossil and paleomagnetic) age reversal from 4.13 Ma to 2.83 Ma is observed at the upper boundary of the fault zone. The lower boundary of this zone was defined at 315 mbsf, and an age reversal from 2.83 Ma to 1.60 Ma is observed across the lower boundary.

[24] The accretionary prism at Site C0008 is located unconformably beneath the slope sediment. Core recovery from the site was very poor but reflection character suggests sandstone-dominated lithology. Their age is unknown but Pliocene is suggested [*Expedition 316 Scientists*, 2009b].

4. Activity and Structure of Shallow Portion of the Splay Fault

[25] The history of splay fault activity and related geologic structures can be inferred from the seismic

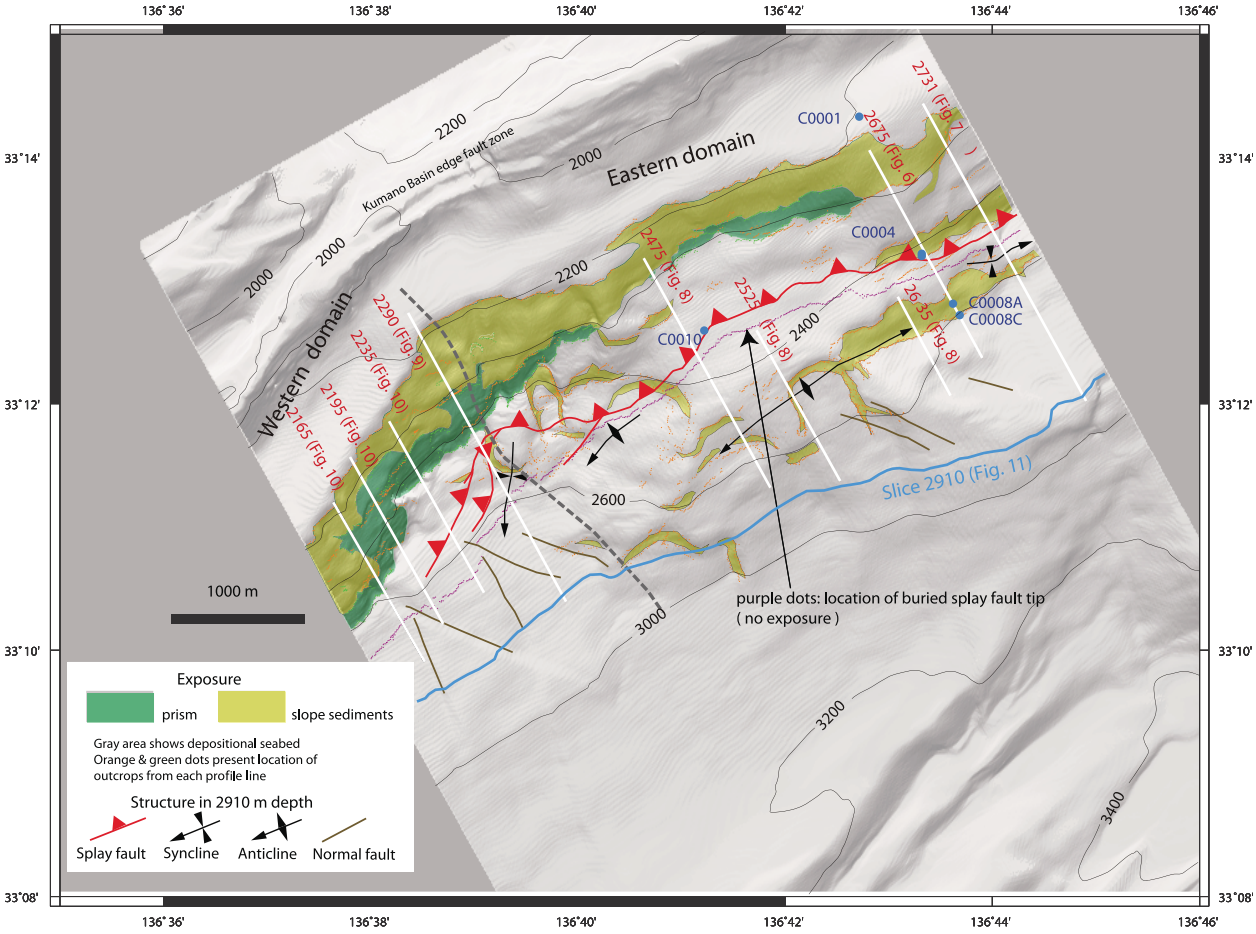

Figure 5. A geological map of the surveyed area. The area is classified into two parts, an erosive area shown by exposures of older bedded sediments and depositional area covered by modern slope sediments. Exposures are subdivided into two, slope sediment exposures and prism outcrops. Most of the exposures are located along steep slopes. Geologic structures on the map of the lower slope basin are reconstructed from 3-D profiles shown in Figures 6 to 11.

data by recognizing the direct link between fault activity and sedimentation and by mapping deformed rocks in the hanging wall and footwall. We present selected type profiles (locations shown on Figure 5) that exhibit clear examples and relations between identified units, key horizons, and structures. Above we subdivided the region into eastern and western domains. The history of splay fault activity appears different in each domain. The ENE striking portion in the eastern domain appears currently active, while activity in the NE trending part in the western domain appears to have ceased. In sections 4.1.1 to 4.1.4, we describe the activity from the selected seismic profiles.

4.1. Splay Fault Activity in the Eastern Domain of Slope

[26] In the eastern domain, five NW trending inline profiles depict the splay fault activity and deformation surrounding the fault. First, we discuss the profile through the drilling sites and then expand the discussion to the east and west in the eastern domain.

4.1.1. Inline 2675

[27] Inline 2675 (Figure 6) is located along a profile connecting drilling Sites C0004 and C0008 (Figure 4). Units Ib and Ic occur as a wedge-shaped package of syntectonic slope basin deposits overlying the accretionary prism.

4.1.1.1. Direct Interaction Between the Faulting and Sedimentation

[28] Thrusts (red lines) cut Units Ib and Ic, and are in turn overlain by the upper part of Units Ib and Ia (Figure 6). Sediments covering the upthrust prism are labeled as Unit Ia on this profile, however,

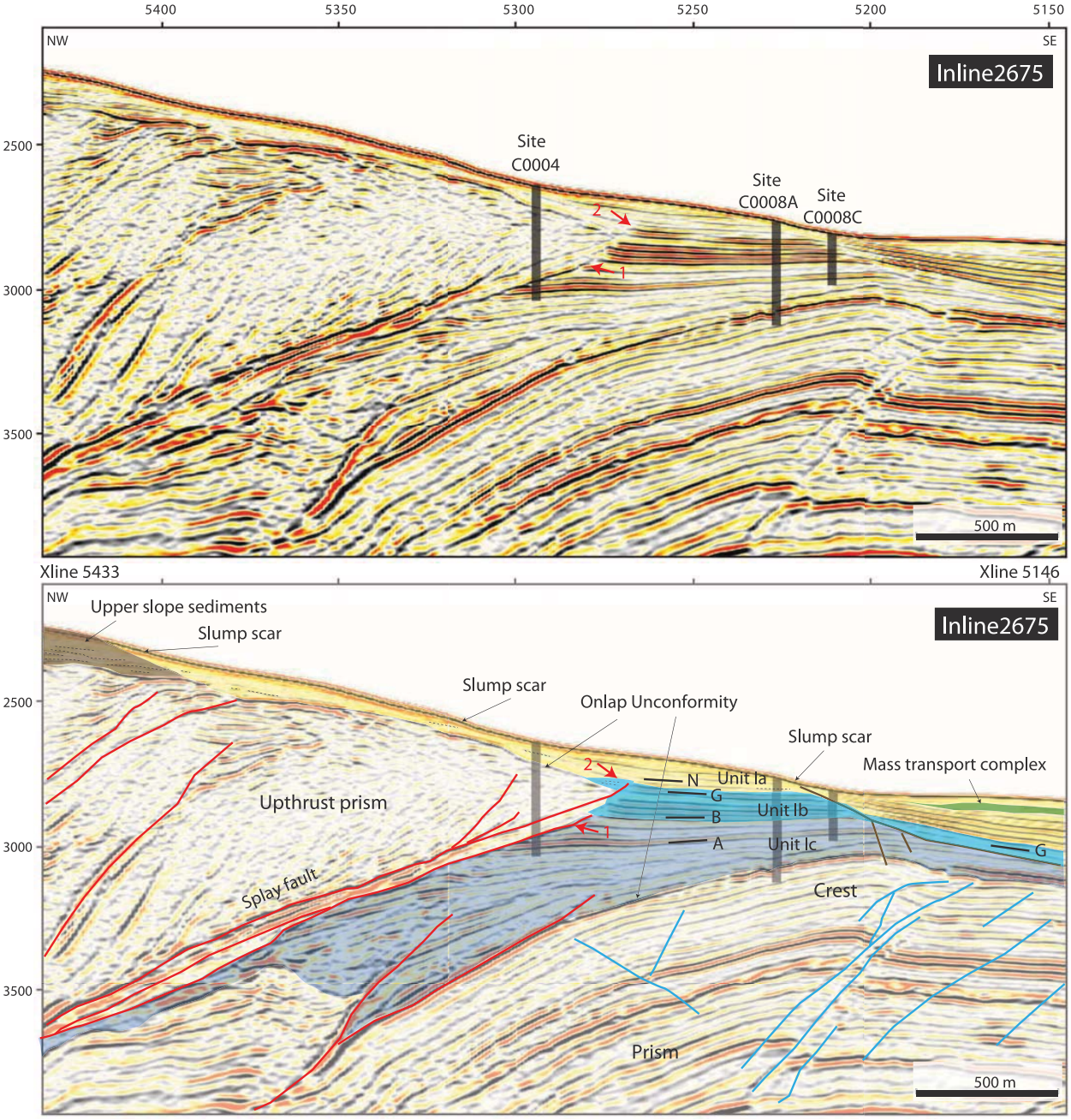

Figure 6. (top) Seismic profile of inline 2675 and (bottom) its interpretation. Location of the line is shown in Figure 5. Horizontal axis is in "XLine," and vertical is depth. Drilling sites are from *Kinoshita et al.* [2009]. Unit colors for interpretation are the same as those in Figure 4. Red lines show branches of splay fault, and blue lines present thrust within the underlying accretionary prism. The letters A, B, G, and N indicate key horizons described in Figure. 4. Detailed interpretation is in the text.

dating of the cores indicates that lowest portion of the sediments includes thin layers age equivalent to Units Ib and Ic (Figure 4). The splay fault kept slipping and cut Unit Ib between 1.55 and 1.24 Ma [*Strasser et al.*, 2009]. The lower boundary of the splay fault zone ceased activity during the deposition of Unit Ib, whereas the upper boundary has remained active well after the 1.24 Ma, as interpreted from the presence of a fault propagation fold observed in the upper part of Unit Ib around the tip of the upthrust accretionary prism sliver (Figure 6). The section of Unit Ia younger than 1.24 Ma is steeply tilted above the prism at Site C0004 (Figure 4) and the shallowest section of the sedi-

ments are dated as being a few thousand to ~70 years old (A. Sakaguchi et al., personal communication). The youngest sediments are composed of mud clast breccias in mud-silt matrix dominated chaotic deposits caused by shaking and slumping. Such deposits are consistent with the occurrence of several slump scars in this area (Figures 2 and 6).

4.1.1.2. Deformation of Footwall

[29] One of the characteristic geologic features on this profile is a low-angle detachment (possibly associated with slumping of shallow, recent slope basin sediments and onlap unconformity) observed to the southeast of Site C0008 (Figure 6). Site C0008C penetrates the shallow portion of this detachment and documents the presence of normal displacement across the feature [*Expedition 316 Scientists*, 2009b] (Figures 4 and 6). The detachment is actually a slip zone with a younger onlap unconformity. Unit Ia thickens beyond this discontinuity (Figure 6), suggesting that slip continued during deposition of Unit Ia.

4.1.2. Inline 2731

[30] Inline 2731 (Figure 7) is located to the east of inline 2675 (Figure 5). The profile shows syndepositional activity of the splay fault and surrounding deformation.

4.1.2.1. Direct Interaction Between Faulting and Sedimentation

[31] Similar to inline 2765, the wedge-shaped packages of Units Ib and Ic indicate that their sedimentation took place concurrently with splay fault displacement and formation of the fault tip anticline. The fault propagation fold developed in sedimentary Unit Ia is clearer on this profile (Figures 7c and 7d) than that on inline 2765. The tip of the splay fault dies out in the upper part of Unit Ib around horizon G and grades into an asymmetric fault propagation anticline that bends Unit Ia upward (Figures 7c and 7d).

4.1.2.2. Deformation of Hanging Wall and Footwall

[32] The following features are especially significant to understanding splay fault activity along this profile. Landslide development affects the sedimentation of Unit Ia and seabed topography. Upper slope sediments deposited on the upthrust prism rocks range in age from ~2 Ma to present (315 Science Party in the study by *Kinoshita et al.* [2009]). They are truncated by a slump scar at the southern edge of the upper slope (Figures 7a and 7b). The sediments displaced by slumping cover upthrust accretionary prism rocks constituting the hanging wall of the splay fault. Two steps characterizing slump scars are recognized on the slope (Figures 7a–7d). Truncation of shallow-level stratification is recognized on the seismic profile, indicating recent slumping activity.

[33] Accretionary prism rocks beneath the splay fault and the slope sediments are deformed into an anticline. Both Units Ib and Ic are thinnest over the crest of anticline and increase in thickness toward the limbs (Figures 7a and 7b). Unit Ia is thicker on the downslope limb of this anticline (Figures 7e and 7f) and onlap is observed around its crest (Figures 7e and 7f). Slump scars are recognized just above the crest of this anticline (Figures 7a, 7b, 7e, and 7f). A low-angle detachment and high-angle normal faults are developed around the crest of the anticline (Figures 7e and 7f). These are restricted in vertical extent, and are found only within the slope sediments and prism rocks directly in and above the crest of this anticline (Figures 7e and 7f). All these features strongly suggest contemporaneous and ongoing anticline formation, faulting, uplift and sedimentation.

4.1.3. Inlines 2635, 2625, and 2475

[34] Inlines 2635 (Figures 8a and 8b), 2525 (Figures 8c and 8d) and 2475 (Figures 8e and 8f) are located to the west of inline 2675 in this order (Figure 5). These profiles mainly show anticline-related deformation outboard of the splay fault. A seabed slump scar, a low-angle detachment with an unconformity, a high-angle normal fault, and minor reverse faults occur around the crest of the anticline.

[35] The seabed slump scar is connected with the underlying low-angle detachment, as well as with a change in thickness of slope sediments. On inline 2525, the seabed slump scar is much gentler than on other inlines, and the change in thickness of Unit Ia beyond the scar appears to be mainly in the lower half of the unit below key horizon N. The low-angle detachment cuts most of Units Ib and Ic and reaches the unconformity boundary between the slope sediments and underlying prism (Figures 8c and 8d). An unconformity is recognized within Unit Ic (Figures 8e and 8f), suggesting an earlier stage of anticline development before ~1.60 Ma (equivalent to horizon A). Another unconformity is also recognized in Unit Ia above key horizon N

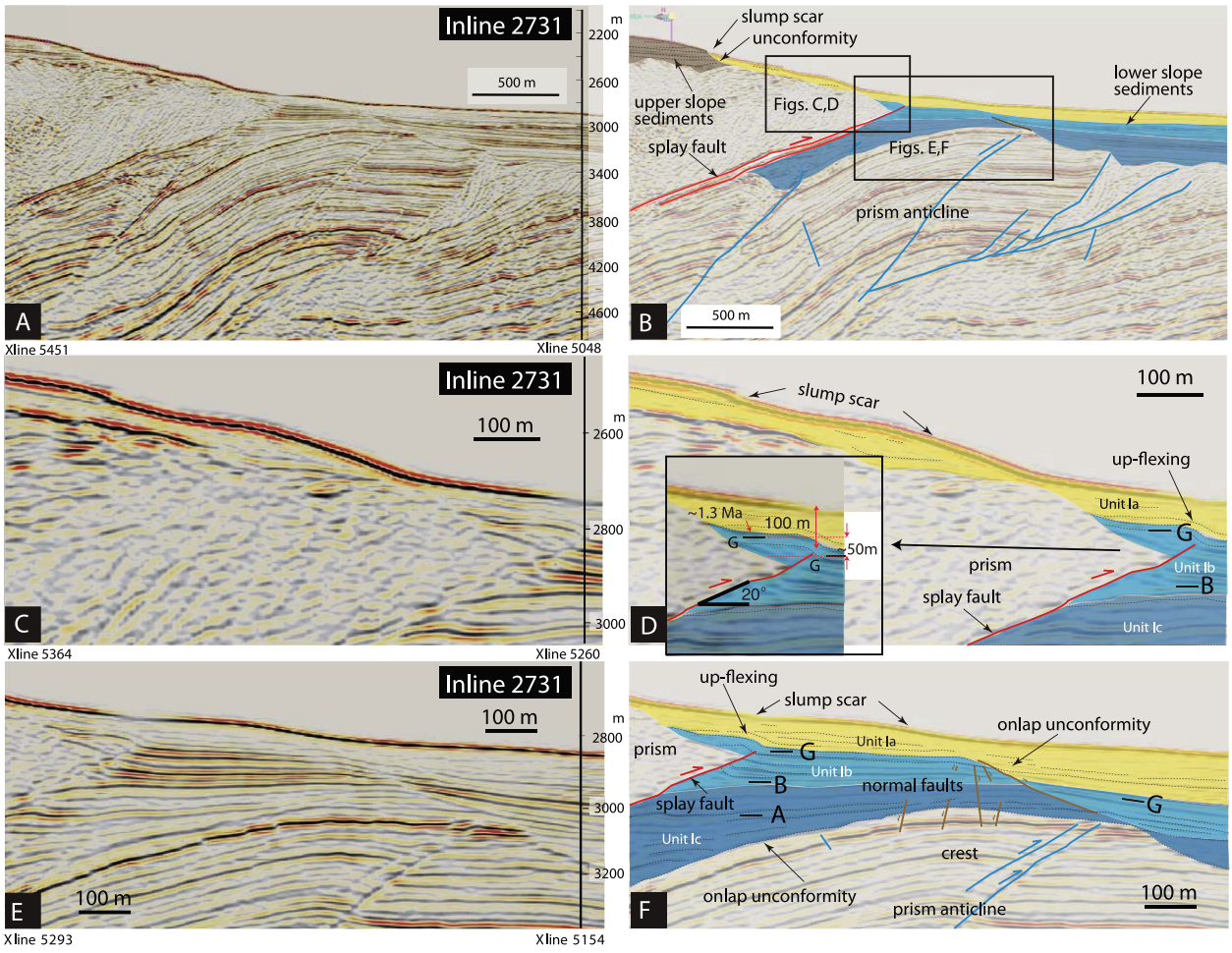

Figure 7. (a, c, e) Seismic profile of inline 2731 and (b, d, f) its interpretation. Location of the line is shown in Figure 5. Red lines show branches of splay fault, and blue lines present thrust within the underlying accretionary prism. The letters A, B, G, and N indicate key horizons described in Figure 4. Horizontal axis is in "XLine" and vertical is depth. Detailed interpretation is in the text.

(Figures 8a, 8b, 8e, and 8f), which indicates an age younger than 1.24 Ma.

[36] High-angle normal faults trending NNW and NW are well-developed mainly in the slope sediments of Units Ib and Ic that are located in the footwall of the detachment. Southward vergent small reverse faults are developed within the folded prism. Their pattern is consistent with the inferred stress field within the crest of an asymmetric anticline, however they do not appear to penetrate into the overlying slope sediments (Figures 8b, 8d, and 8f). The development of both normal and reverse faults associated with the anticline suggests that the neutral surface of the stress field, dividing the local extension in the outside of the fold from compression in the inside of the fold, is located near the top of the anticline in accretionary prism rocks. The extension on the outside of the fold might enhance gravitational collapse of the slope sediments.

[37] On the westernmost profile in the eastern domain of the slope (inline 2475), the splay fault displaces Unit Ic and the lower part of Unit Ib, and transforms to a fault tip anticline in the upper part of Unit Ib (Figures 8e and 8f). Unit Ia (above the anticline) does not appear to be folded in the fault tip anticline, rather it appears to lap onto or drape over the limbs of the anticline (Figures 8e and 8f). No change in the slope of the seafloor is observed above the splay fault. A gentle slump scar is located further up slope, above the upthrust prism (Figures 8e and 8f). These structural features suggest that the splay fault in this region either ceased activity earlier or has not experienced the same degree of displacement over the same time span as further to the east.

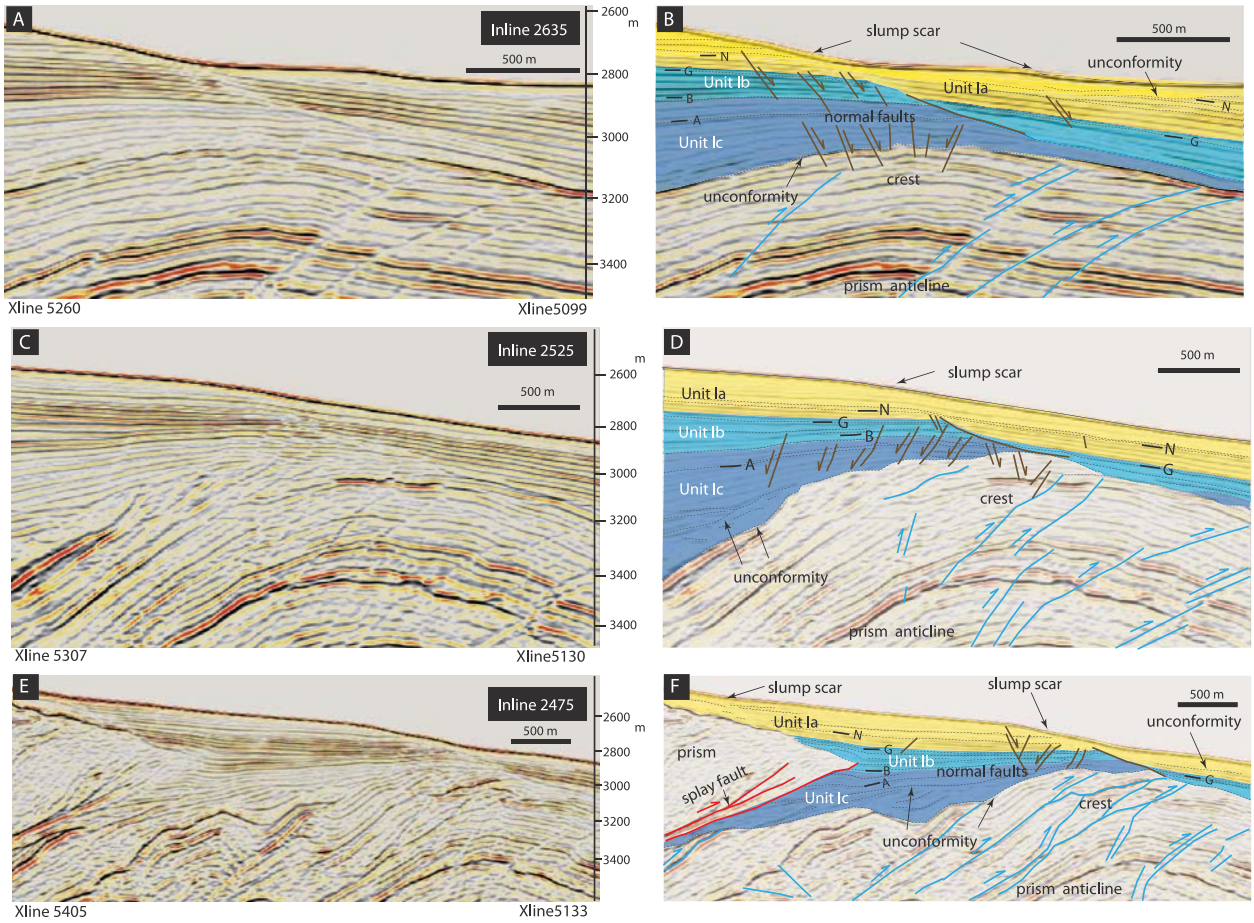

Figure 8. (a, c, e) Seismic profiles of inlines 2475, 2525, and 2635 and (b, d, f) their interpretations showing an anticline of underlying prism and low angle detachment with normal faults mainly in the slope sediments. Locations of the lines are shown in Figure 5. Red lines show branches of splay fault and blue lines present thrust within the underlying accretionary prism. The letters A, B, G, and N indicate key horizons described in Figure 4. Horizontal axis is in "XLine" and vertical is depth. Detailed interpretation is in the text.

4.2. Splay Fault Activity in the Western Domain of Slope

[38] Four profiles from east to west (inlines 2290, 2235, 2195 and 2165), are selected to evaluate the activity of the splay fault in the western slope domain (Figure 5). Direct interaction between faulting and sedimentation, and deformation of host rocks of the hanging wall and footwall are used as criteria. The history of splay fault activity is divided into three phases in this domain; the earliest active phase is documented by activity during deposition of Unit Ic; a second phase shows inactivity mainly by onlap sedimentation of Unit Ib, and the third phase shows reactivation of the fault as indicated by the fault cutting Unit Ib and the overall southward tilting. There is no recent activity after the third phase. These phases are documented from each profile in the following.

4.2.1. Inline 2290

[39] Inline 2290 is located in the easternmost portion of the western domain (Figure 5). Figure 9 shows a profile of the splay fault and the structure of the lower slope basin.

4.2.1.1. Direct Interaction Between Faulting and Sedimentation

[40] Three branches of the splay fault are recognized on the profile (branch A, B, and C in Figure 9). The seaward branch (A) cuts most of Unit Ic and folds the uppermost part of Unit Ic, but is covered by Unit Ib without any later deformation. This observation suggests that activity on branch A ceased before the deposition of Unit Ib (ca. 1.55 Ma) (Figure 9d). The middle branch B of the splay fault thrusts up the prism and offsets the lower half of

Unit Ic but is overlain by the upper part of Unit Ic without any deformation (Figure 9d). The age of key horizon A (ca. 1.60 Ma) suggests that the activity of branch B stopped before that time, and thus prior to cessation of slip on the lower branch (A). The landward fault branch (C) cuts Unit Ic and key horizon B in the lowest portion of Unit Ib (Figure 9d). No fault bend fold is observed in Unit Ib, which onlaps the upthrust prism. This observation suggests that the activity on the upper branch ceased just after 1.55 Ma.

4.2.1.2. Deformation of Hanging Wall and Footwall

[41] Most anticline crests identified in the accretionary prism are simply covered by slope sediments with gentle warping (Figure 9b). One slump scar within Unit Ia is observed on the seabed but neither faults nor folds are recognized beneath that. The timing of the activity of the branches of the splay fault and deformation of the slope sediments suggests no recent displacement or related deformation after ca.1.55 Ma in this area.

4.2.2. Inline 2235

[42] Inline 2235 is located 687.5 m to the west of inline 2290 (Figure 5). The profile (Figures 10a and 10b) exhibits syndepositional deformation different from that of inline 2290.

[43] The splay fault is composed of upper and lower branches, and a branch-and-merge structure is recognized (Figures 10a and 10b). Both the upper and lower branches are bent upward and another fault branches upward from the downward end of the bend (Figures 10a and 10b). The lower branch appears to offset the top of the prism anticline and thrusts these up on to Unit Ic (Figures 10a and 10b). The shallowest portion of the splay fault cuts Units Ic and Ib but is overlain by Unit Ia. No growth structures (such as progressive changes in thickness) beyond the fault or fault bend fold structure are recognized within Unit Ib. This suggests that the splay fault was reactivated after the deposition of Unit Ib, at ~1.24 Ma. Dips of Units Ia appear to increase with aging of the stratigraphic horizon (Figures 10a and 10b), and this occurs in concert with a progressive onlap unconformity over the upthrust prism rocks. The uppermost branch appears to slightly deform Unit Ib and the lower portion of Unit Ia (Figures 10a and 10b). Thus, the most recent activity of the splay fault took place along the uppermost branch. Another feature related to splay fault activity is the deformation of Unit Ic. The wedge shaped package of Unit Ic overlying the footwall prism is folded by a thrust along the base of the sediments (Figures 10a and 10b). The fold is confined within Unit Ic and is overlain by Unit Ib. This indicates that activity on this fault ceased before 1.55 Ma.

[44] These deformation features suggest three phases of activity of the splay fault in this region; an early phase before 1.55 Ma, a second rather quiet phase during the deposition of Unit Ib, and a third phase cutting Unit Ib just after 1.24 Ma. The last phase of activity of uppermost branch of the splay fault was accompanied by trenchward tilting of the entire hanging wall prism.

4.2.3. Inline 2195

[45] Inline 2195 is located 500 m to the west of inline 2235 (Figure 5). The splay fault on this profile is composed of upper and lower branches similar to that identified on inline 2235, however the fault zone is not as thick as in inline 2235 (Figures 10c and 10d). The splay fault is bent upward as well. The bent fault is parallel with stratification of the underlying prism. The upper branch of the splay fault offsets and folds Unit Ib. Kink-like bending is not limited to Unit Ib but also appears to control the geometry of the lower part of Unit Ia just below key horizon N on this profile (Figures 10c and 10d). Sediments above key horizon N exhibit an onlap unconformity. The thickness of the sedimentary package beyond the kink and thrust does not change and stratal dip angles are constant, suggesting that thrusting and kinking occurred just after deposition. The history of the splay fault on this profile is reconstructed as follows: earliest thrusting coincident with deposition of Unit Ic, quiescence during the deposition of Unit Ib, reactivation of thrusting just after the deposition of Unit Ib and the lower part of Unit Ia. Bending of the splay fault appears to have taken place together with the growth of the anticline observed in the underlying accretionary prism.

4.2.4. Inline 2165

[46] Inline 2165 is located 375 m to the west of inline 2195 (Figure 4). This profile resembles inline 2195 in general, but is slightly different in detail. The splay fault zone is thinner than that on inline 2195 and branches only near the tip of the fault. The displacement along the splay fault is limited to the period of Unit Ic deposition (Figures 10e and 10f). Unit Ib and the lower part of Unit Ia below

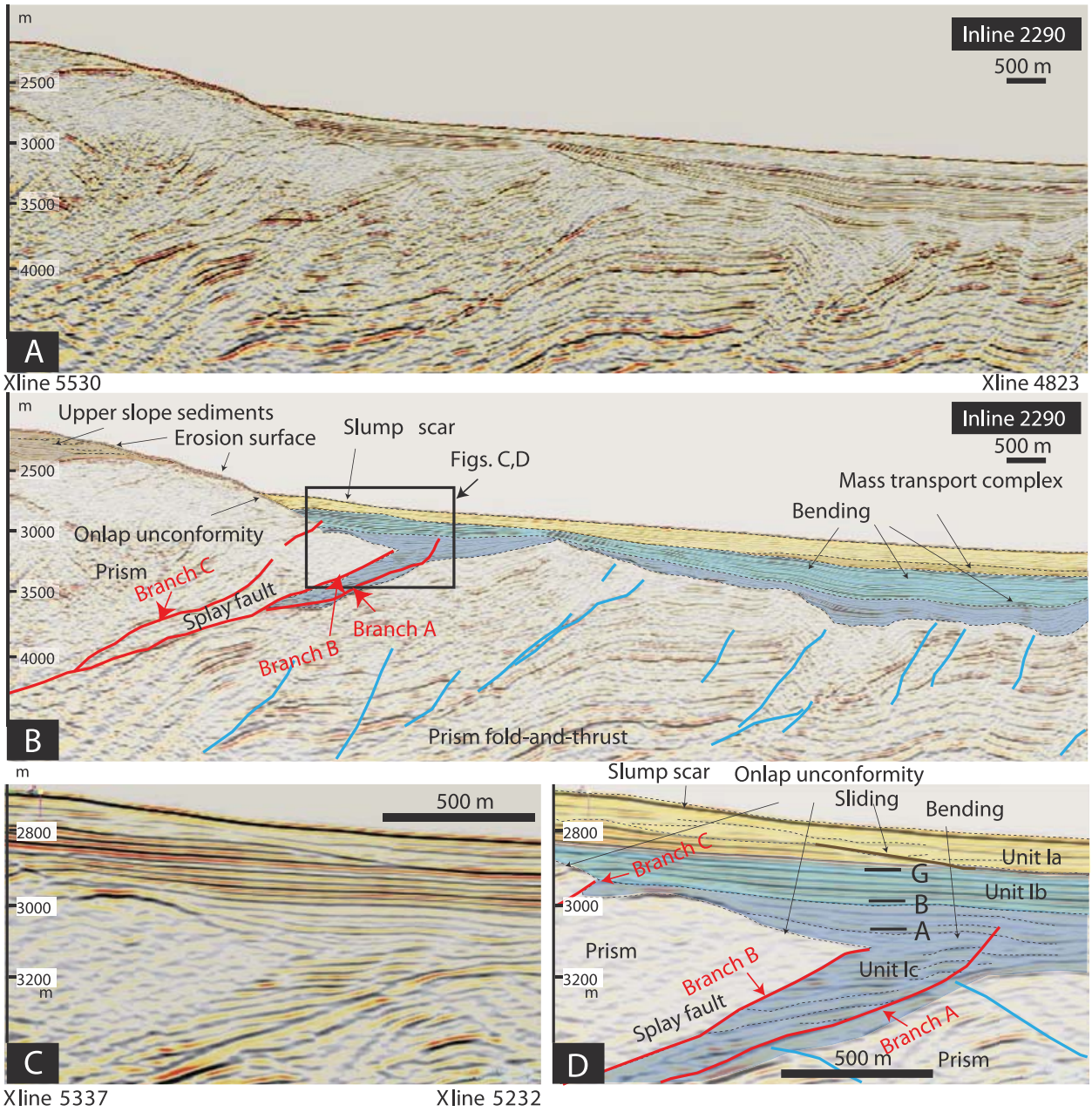

Figure 9. (a) Seismic profile of inline 2290 and (b) its interpretation. (c, d) A close-up profile and its interpretation around the tip of the splay fault, respectively. Location of the line is shown in Figure 5. Red lines show branches of splay fault and blue lines present thrust within the underlying accretionary prism. The letters A, B, G, and N indicate key horizons described in Figure 4. Horizontal axis is in "XLine," and vertical is depth. Detailed interpretation is in the text.

key horizon N exhibit trenchward tilting to a final dip angle steeper than that on inline 2195. Units Ib and Ia onlap the upthrust prism. A slight bending is recognized in the lower portion of Unit Ia above the prism. Inferred tectonic activity on this profile is almost the same as that on inline 2195 except that 2165 does not include reactivation after the deposition of Unit Ib.

4.3. Structural Variation and Surface Geology

[47] Figure 11 presents a horizontal depth slice at 2910 m below sea level (see Figure 4 for location). This slice reveals the geologic structure of the lower slope basin very well on the basis of tracing key horizons A to N and Unit Ia to Ic (Figure 11).

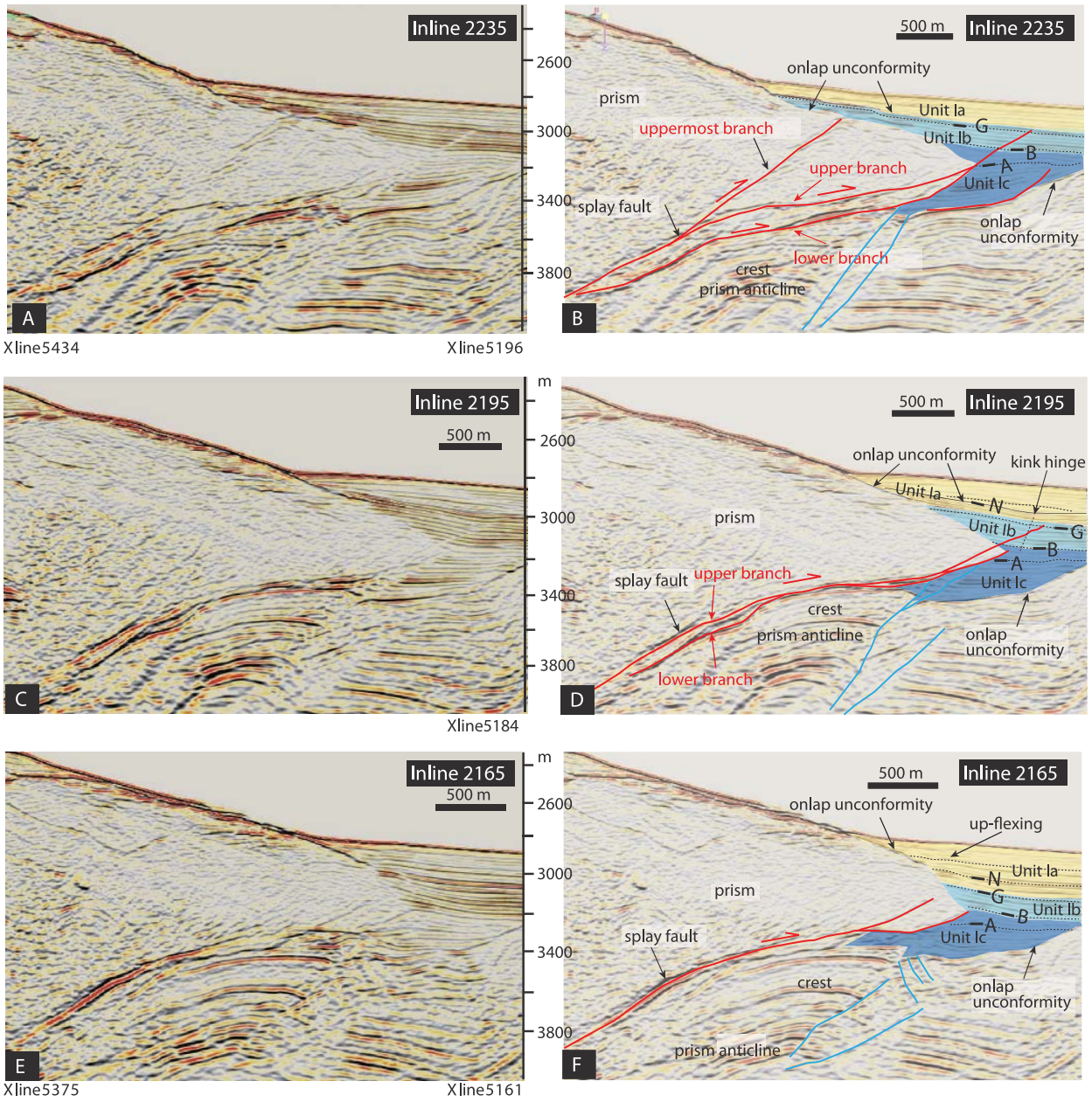

Figure 10. (a, c, e) Seismic profiles of inlines 2235, 2195, and 2165 and (b, d, f) their interpretations showing anticline of underlying prism and low angle detachment with normal faults mainly in the slope sediments. Locations of the lines are shown in Figure 5. Red lines show branches of splay fault, and blue lines present thrust within the underlying accretionary prism. The letters A, B, G, and N indicate key horizons described in Figure 4. Horizontal axis is in "XLine", and vertical is depth. Detailed interpretation is in the text.

The splay fault strikes ENE in the eastern domain but its strike changes and branches to the NE in the western domain as described in sections 4.1 and 4.2 (Figure 11). A 3-D image of the splay fault with a horizontal slice at a depth of 4336 m below sea level is displayed in Figure 12 as a view from the bottom. The fault surface is not smooth, but is rough in many places. Such roughness of the splay fault appears to be related to deformation of the hanging wall and footwall blocks. Depth slice 4330 shows the deformation of the accretionary prism underlying the slope sediments. A structural contrast of slope sediments and accretionary prism in eastern and western domains is clearly recognized as follows.

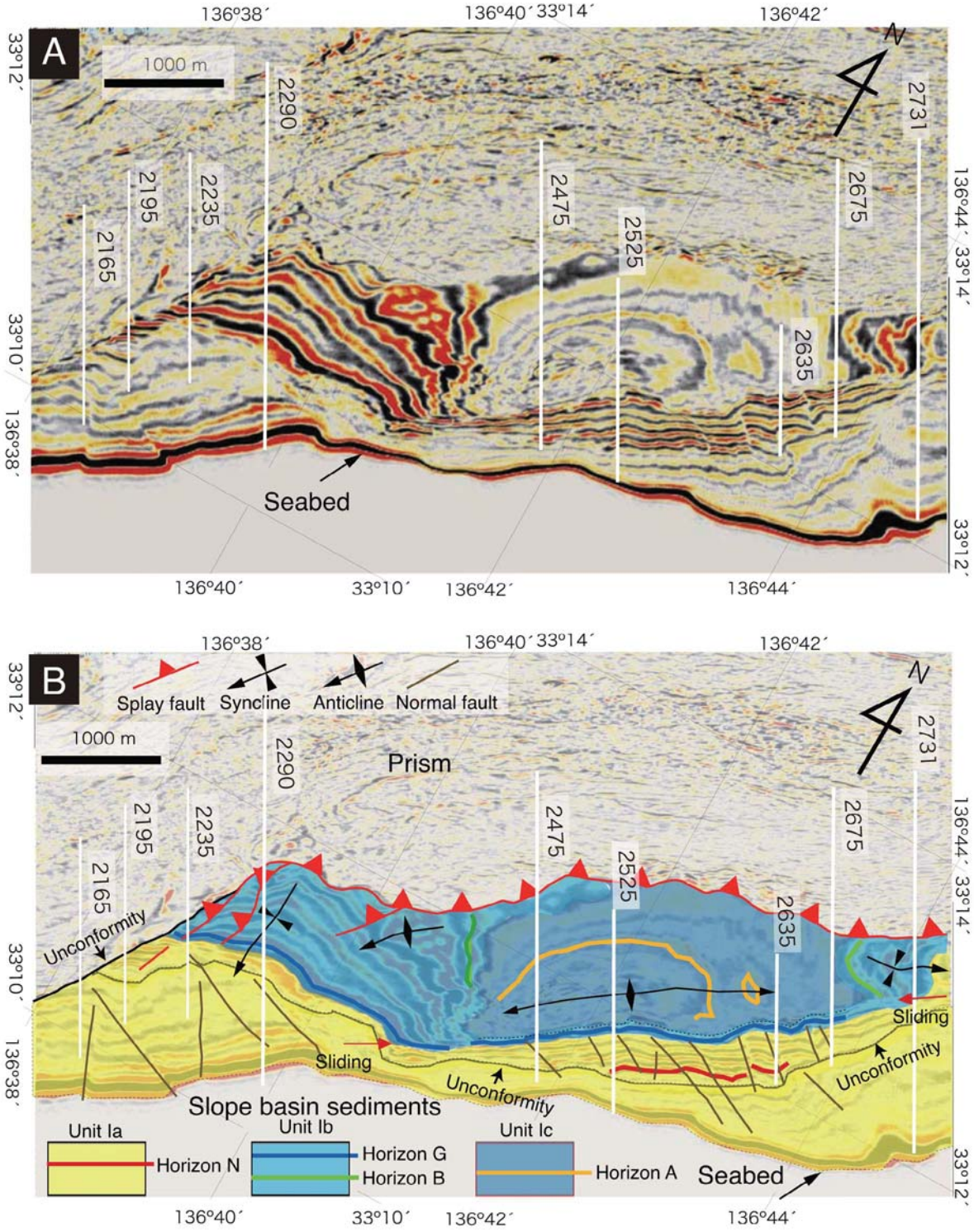

Figure 11. Horizontal seismic profile of (a) slice 2910 and (b) geological interpretation showing a structure of the slope sediments. Location of the slice is shown in Figure 5. The letters A, B, G, and N indicate key horizons described in Figure 4. Detailed interpretation is in the text.

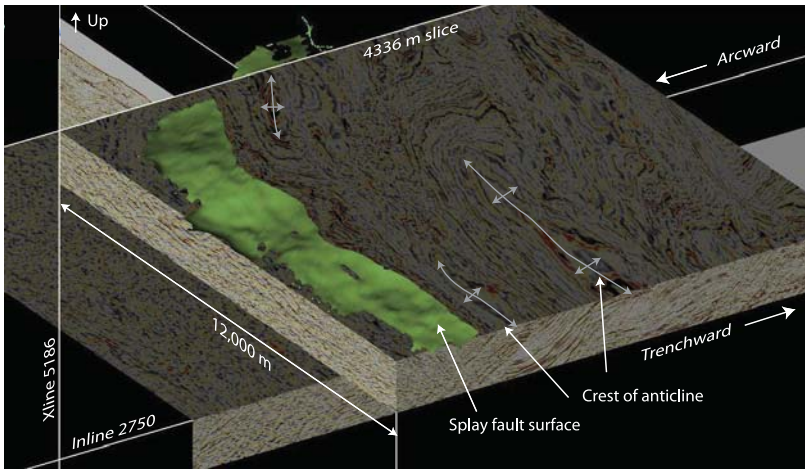

Figure 12. Horizontal seismic slice at 4336 m with the splay fault surface. Traces of crests of anticlines of accretionary prism underlying in the footwall of the splay fault are also shown.

4.3.1. Structure of the Slope Sediments and Surface Geology

[48] Deformation of slope sediments in the eastern domain is characterized by an ENE elongate, dome-like anticline (Figures 11a and 11b). The northern wing of the anticline has a gentler dip than the southern limb and is thrust up by the splay fault. The southern limb of the anticline undergoes a gradual decrease in dip toward the south, away from the axis of the anticline. A syncline with its axis parallel to the ENE strike of the splay fault is observed in the easternmost part of the slope basin (Figure 11). A southward dipping monocline is identified in the western domain of the slope basin. A gentle N-S trending syncline and a NE trending anticline are observed near the splay fault around the border of the eastern and western domains. The uppermost part of Unit Ia in the slope sediments gently dips to the SSE and is cut by NW and NNW trending high-angle faults (Figure 11). These are interpreted to be primarily normal faults with a slight strike-slip component which are consistent with present stress field observed from borehole breakouts, fractures in cores, and anelastic strain recovery of the cores [*Byrne et al.*, 2009]. The NW and NNW trending faults are primarily confined to Unit Ia. A regional unconformity is recognized within Unit Ia above key horizon N (Figure 11b). The age of this unconformity appears to be younger than 1 Ma based on magnetostratigraphy [*Strasser et al.*, 2009]. These structures of the slope sediments are clearly reflected in the surface topography and geology (Figure 4). Landslide heads in the eastern domain trend ENE along the crest of the dome-like anticline (Figure 4) indicate their recent activity. The topographic variation between the eastern and western domains is the result of the deformation of the slope sediments.

4.3.2. Deformation of the Accretionary Prism

[49] Inline profiles described previously (section 4.1) show syndepositional growth of an anticline beneath the slope basin sediments. The horizontal slice at 4330 m depth, together with the profiles, demonstrates the 3-D features of the anticline together with fine deformational aspects of the accretionary prism (Figure 12). Axes of three dome-like anticlines are parallel to the strike of the splay fault. Domes are separately formed in both eastern and western domains (Figure 12). These folds appear to control the deformation and sedimentation of the slope basin above the accretionary prism. Thus, the splay fault movement, deformation of the hanging wall of the accretionary prism, and slope basin development are all linked to each other.

4.4. Summary of Activity of the Splay Fault and Surrounding Deformation

[50] Detailed investigation of the three dimensional structure of the shallow portions of the splay fault and associated deformation of sediments defining the lower slope basin reveal the temporally and spatially dependent variations in fault slip and fault evolution. The ENE striking, eastern portion of the splay fault has remained active since the inception of faulting at ~1.95 Ma [*Strasser et al.*, 2009]. Early activity is interpreted to represent in-sequence thrusting that evolved to out-of-sequence (splay

fault) thrusting [*Strasser et al.*, 2009]. Rapid synsedimentary uplift of the prism rocks in the hanging wall of the splay fault is recorded from 1.55 and 1.24 Ma. After 1.24 Ma, activity of the splay fault is recorded not only by stratal ages and architecture, but also in the erosion and redeposition of slope sediments by successive oversteepening, mass transport, formation of slump scars, and accumulation of mass transport deposits overlying the fault. The active strand of the splay fault zone identified in inline 2675 shifted to the upper branch at ~1.55 Ma [*Expedition 316 Scientists*, 2009a; *Strasser et al.*, 2009]. This activity is expressed along the splay fault itself (as inferred from offset sedimentary units), and by broader and distributed deformation, especially deformation of the lower slope basin. An ENE striking, elongated anticline is developed in the accretionary prism together with folding of slope sediments in the footwall of the splay fault. A low-angle detachment located near the crest of the anticline forms the slip surface along which slumping occurs, as shown by the location of seafloor slump scars, incipient headwall scarps, and the distribution of abundant mass transport deposits in the slope basin. NW trending and WNW trending normal faults cut the crest of the anticline and folded slope basin sediments. These features indicate that the folding is currently active and is related to the splay fault activity. Coseismic slip along the splay fault may induce collapse along the limbs of this anticline due to seabed shaking and enhanced gravitational instability of a wide area around the splay fault.

[51] The strike of the western portion of the splay fault changes to the NE and exhibits a different mode of activity. Early stage activity before 1.55 Ma may have been similar to that described for the eastern portion. For the period between 1.55 and 1.24 Ma, we infer relative quiescence based on the constant thickness of Unit Ib in the area. During this period, the splay fault itself may have been bent together with the footwall accretionary prism. The modification of the splay fault dip angle may have prevented slip. This change in original fault geometry may have precipitated the formation of a secondary branch of the splay fault cutting through the previously developed fault propagation anticline and into younger slope sediments (the shallower portions of Unit Ib), as observed in inline 2235. Splay fault activity again ceased after formation of the secondary branch, as suggested by unconformable onlapping of Unit Ia sediments over the faulted and folded sediments of Unit Ib, blanketing of faults and scarps by recent sediments, and regional low-intensity tilting without displacement. We suggest that this portion of the splay fault has been inactive over the last 1.24 Ma, and that the NE striking portion of the splay fault has undergone regional uplift or tilting, perhaps related to drag during slip along faults identified further landward as suggested by *Moore et al.* [2007].

[52] Comparison of offset and other deformation features along the fault and in the affected slope basins suggests a gradual decrease in slip rate from 1.55 Ma to Recent [*Strasser et al.*, 2009]. Although the average slip rate along the splay fault appears to decrease, this does not require that the deeper portion of the splay fault underwent a similar change in slip rate, rather, we infer that slip along the deeper sections of the splay fault was accommodated by formation of fault propagation anticlines and more distributed deformation in the slope basin.

5. Discussion

[53] We discuss three points in sections 5.1 to 5.3: synsedimentary activity of the splay fault, partitioning of plate convergence slip, and the space-time evolution of the splay fault in a regional tectonic framework with special emphasis on seamount collision.

5.1. Synsedimentary Activity of the Splay Fault

[54] Seismic profiles described in sections 4.1 and 4.2 show that, rather than a simple intersection between the fault tip and the seafloor, there is a complex interaction between fault propagation folding, seafloor slumping and sliding, faulting and deformation of shallow strata, and widespread deposition of mass transport deposits and debris slides. These features are distinct from those of seismically active thrust faults on land in general, but are very significant indicators of the style and degree of activity of this submarine thrust fault system, particularly with respect to similar systems in other subduction zones.

[55] Landslides, slumps, and mass transport deposits around the splay fault are observed and well documented, especially along the eastern portion of the splay fault as described above. The slope angle adjacent to the slide is ~4°and the slump scars dip ~6°–8°. This suggests that the slope is at or near the critical angle and slight tilting and/or shaking could trigger sliding or slumping events. In the case of

muddy, soft, highly porous and uncompacted sediments, the same critical angle is well observed and documented in the Gulf of Mexico [e.g., *Sawyer et al.*, 2009]. The rather gentle angle of the slump scars appears to be related to the strength or angle of internal friction of the muddy sediments. Most of the mechanical data available for these materials with as much as ~60%–70% porosity, however, would suggest that the coefficient of friction is too high to fail at such low angles. Therefore, high pore fluid pressure and/or ground shaking are necessary to trigger the landslides.

[56] Nannofossil populations of Units Ia and Ib exhibit significant mixing of older and younger fossil assemblages, probably related to debris flow deposits (Expedition 316 Scientists in the study by *Kinoshita et al.* [2009]), suggesting that muddy deposits on the footwall side of the fault propagation anticline may be composed mainly of mass transport deposits containing reworked material from upslope. We suggest that these slump features are an inherent reflection of the distributed deformation related to slip along the splay fault, as slip is accommodated by formation of the anticline and soft, recent sediments are oversteepened and/or shaken by periodic earthquakes. One of the targets of NantroSEIZE stage 2 drilling is to document the factors that control the landslides [*Henry et al.*, 2010].

5.2. Slip Partition of Plate Convergence

[57] Syndepositional activity is inferred in terms of the balance between the vertical throw rate of the splay fault and measured or inferred local sedimentation rates. Inline 2731 (Figure 7d) shows that most of Unit Ib is displaced by the splay fault, however the uppermost part of Unit Ib and all of Unit Ia are folded into a gentle anticline, rather than being offset along the fault. The amount of bending gradually decreases upward and grades into a gentle step on the seabed formed by a slump scar. A layer dated at ~1.30 Ma in the uppermost part of Unit Ib is bent and the vertical throw due to this bending is ~50 m (Figure 7d), therefore the averaged vertical throw rate is ~0.04 m/kyr. On the other hand, the combined thickness of the uppermost part of Unit Ib and Unit Ia is ~100 m, requiring a sedimentation rate of ~0.08 m/kyr, twice the vertical throw rate (Figure 7d). This vertical throw rate is converted to a horizontal shortening rate of ~1 m/kyr because the dip angle of the splay fault is ~20° (Figure 7d). The horizontal shortening rate is ~1.5%–2.5% of the total plate convergence of ~40–65 m/kyr. Thus the partitioning of plate convergence along the splay fault is very small on average. Other parts of the total slip might consist of internal deformation of the accretionary prism and slip along the basal décollement itself. *Screaton et al.* [2009] estimated that the shortening due to slip along to the frontal thrust reaches 13% to 34% of the plate convergence during activity between ~0.436 and 0.78 Ma and the present. They could not estimate the partitioning of convergence along the imbricate thrust zone or other portions of the frontal thrust zone because there is no age control. It is, however, obvious that significant amount of shortening exists within these zones and contributes to the plate convergence much larger than that along the described branch of the megasplay fault. *Sakaguchi et al.* [2011] reported that fault gouges and their surrounding hosts from the splay fault (C0004) and frontal thrust (C0007, Figure 1) show frictional heating, suggesting high-velocity slip. Low-frequency earthquakes document activity along the splay fault and thrusts within the imbricate thrust zone in the Nankai Trough [*Obana and Kodaira*, 2009]. These facts and broadly observed deformation challenge the commonly accepted idea that megasplay fault (or out-of-sequence thrust) bounding inner and outer wedges acts as the primary plate boundary and accommodates all coseismic slip; the outer wedge then slips and deforms in response to this during the postseismic period [*Wang and Hu*, 2006]. The outer wedge is deformed not only during the post seismic period but may also be deformed coseismically together with the slip along the splay fault and may contribute to tsunamigenesis. Further research is necessary, however, to quantify spatial and temporal variation in slip partitioning.

5.3. Splay Fault Activity With Respect to a Seamount Collision

[58] The difference in activity between the eastern and western domains of the splay fault might extend to a more regional-scale interpretation. Figures 1b and 13 show the regional-scale topography of the fore-arc and accretionary prism. To the southeast of the investigated area, there are regions of imbricate and frontal thrust zones (Figure 2). Axial traces of anticlines and strikes of thrusts in the imbricate thrust zone trend NE, which is almost normal to the relative plate convergence direction, whereas those in the younger frontal thrust zone trend ENE and oblique to the plate convergence (Figures 2 and 13). The reason for the change in the orientation from NE to ENE may be

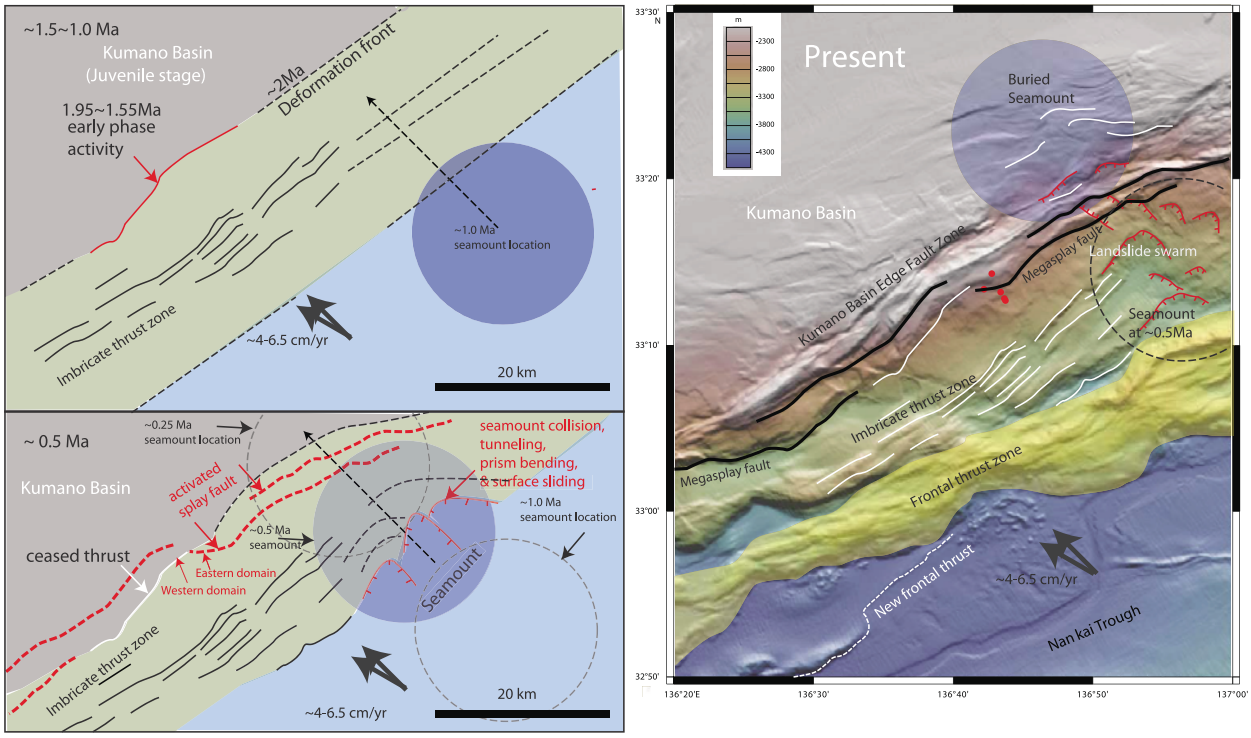

Figure 13. A cartoon showing a tectonics process of seamount collision and deformation of the forearc at ~1.55–1.0 Ma, 0.5 Ma, and present. Previous locations of the seamount are also shown based on the minimum plate convergent rate (~4.0 cm/yr) and its direction.

explained by a change in relative convergence direction, and/or a modification of the prism architecture caused by collision of obstacles (such as seamounts), and/or initiation of oblique subduction during the period between the imbricate thrust and the frontal thrust zones.

[59] As the splay fault was initially a frontal thrust at 1.95 Ma [*Strasser et al.*, 2009], all of the accretionary prism outboard of the splay fault might be younger than that age. Relative plate convergence between the Philippine Sea plate and southwest Japan is inferred to have changed drastically at ~3–5 Ma on the basis of onland geologic phenomena [*Kimura et al.*, 2005; *Takahashi*, 2006] and beginning of tearing of the Philippine Sea plate [*Ide et al.*, 2010], but no significant change has been inferred since that time. Therefore, the change in strikes of the thrusts from NE in the imbricate thrust zone to ENE in the frontal thrust zone cannot be ascribed to a change in relative plate convergence.

[60] To the east of the investigated area, a topographic high (Figure 13) is inferred to reflect a subducted seamount associated with fossil indentation to the south [*Kington and Tobin*, 2009]. The fossil indentation and associated development of landslides are observed only in the imbricate thrust zone (Figure 13). This suggests that the collision might have started during the development of the imbricate thrust zone and may have finished before the development of present frontal thrust zone (Figure 13). Reconstructing the seamount back to its position prior to 1 Ma on the basis of the present minimum convergence rate of ~4 cm/yr, shows that it was located outboard of the imbricate thrust zone (Figure 13), was subducted beneath the imbricate thrust zone after that time, and is now located to the north of the splay fault and KBEFZ (Figure 13). The architecture of the accretionary prism was likely modified by a seamount collision and subduction, similar to that observed in the Nankai trough off the Muroto Peninsula [e.g., *Moore et al.*, 2007]. The splay fault activity in the early phase stopped in the western domain after 1.55 Ma. The splay fault bent together with continuous growth of footwall accretionary prism in the imbricate thrust as described in section 4.2. Such geometrical modification of the splay fault may have prevented its activity and enhanced regional uplift. Before the formation of the frontal thrust zone, a thick, seismically transparent layer was underplated beneath the imbricate thrust zone [*Park et al.*, 2010]. All

these events appear to have taken place together with the seamount collision.

[61] Old large landslides in the imbricate thrust zone are cut by the young ENE trending splay fault and KBEFZ (Figure 13) to the south of the buried seamounts [*Kington and Tobin*, 2009]. KBEFZ is composed mainly of normal faults and dextral strike-slip faults behind the megasplay fault [*Martin et al.*, 2010]. The KBFEZ and the splay fault strike almost parallel to the frontal thrust zone and to the present deformation front, which is modified by indentation due to recent collision of rather small seamounts [*Moore et al.*, 2009] (Figure 13). Deformation of the frontal thrust zone, active splay fault, and KBEFZ with a dextral strike-slip component, suggests that oblique subduction may have been enhanced after the indentation of the large seamount in the imbricate thrust zone. The ENE trending splay fault in the eastern domain of the surveyed area is located at the western end of the segment to the south of the buried seamount (Figure 13) and remains active in contrast to that in the western domain. Continuous activity of the eastern domain of the splay fault after 1.24 Ma may be related to geometrical adjustment due to reorientation of the fault after the seamount passed beneath the imbricate thrust zone. Recent enhancement of oblique subduction may be linked to increased activity in KBEFZ and the splay fault that decouples the outer wedge from the inner wedge beneath the Kumano fore-arc basin and much larger-scale activity as shown in rapid mountain building and active faulting on land after ~1 Ma [*Research Group for Active Faults*, 1991; *Ikeda et al.*, 2009] and recent clear tearing of the Philippine Sea plate [*Ide et al.*, 2010]. Many studies have inferred that coseismic slip along splay faults that branch from the plate boundary megathrust may provide a mechanism by which earthquakes generate tsunamis [*Fukao*, 1979; *Plafker*, 1972; *Baba et al.*, 2006; *Tanioka and Satake*, 2001]. A complicated evolving process of the splay fault in the Nankai trough shown in this paper may give a clue to reveal individual characteristics of the splay faults and evaluate their activities in each subduction zone.

6. Conclusion

[62] We investigated the three-dimensional structure of the shallow portions of the splay fault combined with the results of drilling and dating of IODP core during the NantroSEIZE project to define the spatial and temporal evolution of the splay fault in the Kumano area, Nankai Trough, off southwest Japan. In the investigated area, the splay fault and surface topography is divided into eastern and western domains. The differences between domains: geometry, activity and surface manifestations, result from differences in evolving processes, which may depend on a slight difference of distance from the location of a collided and subducted seamount and interaction between fault slip and sedimentation. Complicated and evolving processes of the accretionary prism determined the location of the splay fault as the boundary between the inner and outer wedges. The megasplay started to function as a seismogenic fault during large earthquakes along this margin, but the slip partition of the shallow portion of the fault is only ~1.5%–2.5% of the total plate convergence. This fact suggests that branches of the megasplay fault and outer wedge may slip and deform coseismically. The investigated and drilled area is limited, but the clarified details of the evolving process may apply to the entire splay fault system in the Nankai trough and other margins. The orientation and geometry of the splay fault are keys to evaluate the activity in general that may contribute to assessment of seismic and tsunami hazards in the future.

Acknowledgments

[63] The authors thank the ship and drilling personnel, staff, and technicians aboard the D/V *Chikyu* and the Center for Deep Earth Exploration (CDEX) for their work that allowed the overall success of the expedition. The authors also thank NantroSEIZE scientists of Expedition 316 (F. Chester, O. Fabbri, C. Fergusson, F. Girault, D. Goldsby, R. Harris, F. Inagaki, T. Jiang, Y. Kitamura, M. Knuth, C.-F. Li, L. Claesson Liljedahl, L. Louis, K. Milliken, U. Nicholson, N. Riedinger, A.Sakaguchi, E.Solomon, X. Su, A. Tsutsumi, K. Ujiie, A. Yamaguchi, and X. Zhao). Comments by Demian Saffer and two anonymous reviewers greatly improved this paper. This research used samples and data provided by the Integrated Ocean Drilling Program (IODP) and is supported by grant-in-aid by MEXT-KAKENHI 21107005 and NSF grant OCE-0451790. We thank Paradigm for providing the seismic interpretation software used in this study.

References

Ando, M. (1975), Source mechanisms and tectonic significance of historical earthquakes along the Nankai trough, Japan, *Tectonophysics*, *27*, 119–140, doi:10.1016/0040-1951(75)90102-X.

Aoki, Y., T. Tamano, and S. Kato (1982), Detailed structure of the Nankai Trough from migrated seismic sections, in *Studies in Continental Margin Geology*, edited by J. S. Watkins and C. L. Drake, *AAPG Mem.*, 34 309–322.

Ashi, J., et al. (2002), Structure and cold seep of the Nankai accretionary prism off Kumano—Outline of the off Kumano survey during YK01-04 Leg 2 Cruise, JAMSTEC *J. Deep Sea Res.*, *20*, 1–8.

Baba, T., and P. R. Cummins (2005), Contiguous rupture areas of two Nankai Trough earthquakes revealed by high-resolution tsunami waveform inversion, *Geophys. Res. Lett.*, *32*, L08305, doi:10.1029/2004GL022320.

Baba, T., P. R. Cummins, T. Hori, and Y. Kaneda (2006), High precision slip distribution of the 1944 Tonankai earthquake inferred from tsunami waveforms: Possible slip on a splay fault, *Tectonophysics*, *426*, 119–134, doi:10.1016/j.tecto.2006.02.015.

Bangs, N. L. B., G. F. Moore, S. P. S. Gulick, E. M. Pangborn, and H. Tobin (2009), Broad, weak regions of the Nankai Megathrust and implications for shallow coseismic slip, *Earth Planet. Sci. Lett.*, *284*, 44–49, doi:10.1016/j.epsl.2009.04.026.

Byrne, T. B., W. Lin, A. Tsutsumi, Y. Yamamoto, J. C. Lewis, K. Kanagawa, Y. Kitamura, A. Yamaguchi, and G. Kimura (2009), Anelastic strain recovery reveals extension across SW Japan subduction zone, *Geophys. Res. Lett.*, *36*, L23310, doi:10.1029/2009GL040749.

Expedition 314 Scientists (2009), Expedition 314 Site C0004, in *NanTroSEIZE Stage 1: Investigations of Seismogenesis, Nankai Trough, Japan*, *Proc. Integr. Ocean Drill. Program*, 314/315/316, doi:10.2204/iodp.proc.314315316.116.2009.

Expedition 316 Scientists (2009a), Expedition 316 Site C0008, in *NanTroSEIZE Stage 1: Investigations of Seismogenesis, Nankai Trough, Japan*, *Proc. Integr. Ocean Drill. Program*, 314/315/316, doi:10.2204/iodp.proc.314315316.136.2009.

Expedition 316 Scientists (2009b), Expedition 316 Site C0004, in *NanTroSEIZE Stage 1: Investigations of Seismogenesis, Nankai Trough, Japan*, *Proc. Integr. Ocean Drill. Program*, 314/315/316, doi:10.2204/iodp.proc.314315316.133.2009.

Fukao, Y. (1979), Tsunami earthquakes and subduction processes near deep-sea trenches, *J. Geophys. Res.*, *84*, 2303–2314, doi:10.1029/JB084iB05p02303.

Henry, P., T. Kanamatsu, and M. Kyaw Thu (2010), NanTroSEIZE Stage 2: Subduction inputs 2 and heat flow, *Integr. Ocean Drill. Program Sci. Prospectus.*, *333*, doi:10.2204/iodp.sp.333.2010.

Ide, S., K. Shiomi, K. Mochizuki, T. Tonegawa, and G. Kimura (2010), Split Philippine Sea plate beneath Japan, *Geophys. Res. Lett.*, *37*, L21304, doi:10.1029/2010GL044585.

Ike, T., G. F. Moore, S. Kuramoto, J. O. Park, Y. Kaneda, and A. Taira (2008), Variations in sediment thickness and type along the northern Philippine Sea plate at the Nankai Trough, *Isl. Arc*, *17*, 342–357, doi:10.1111/j.1440-1738.2008.00624.x.

Ikeda, M., S. Toda, S. Kobayashi, Y. Ohno, N. Nishizawa, and I. Ohno (2009), Tectonic model and fault segmentation of the Median Tectonic Line active fault system on Shikoku, Japan, *Tectonics*, *28*, TC5006, doi:10.1029/2008TC002349.

Kame, N., J. R. Rice, and R. Dmowska (2003), Effects of prestress state and rupture velocity on dynamic fault branching, *J. Geophys. Res.*, *108*(B5), 2265, doi:10.1029/2002JB002189.

Karig, D. E., et al. (1975), *Initial Reports of the Deep Sea Drilling Project*, 31, U.S. Govt. Print. Off., Washington, D. C., doi:10.2973/dsdp.proc.31.1975.

Kikuchi, M., M. Nakamura, and K. Yoshikawa (2003), Source rupture processes of the 1944 Tonankai earthquake and the 1945 Mikawa earthquake derived from low-gain seismograms, *Earth Planets Space*, *55*, 159–172.

Kimura, J., R. J. Stern, and T. Yoshida (2005), Reinitiation of subduction and magmatic responses in SW Japan during Neogene time, *Geol. Soc. Am. Bull.*, *117*, 969–986, doi:10.1130/B25565.1.

Kimura, G., Y. Kitamura, Y. Hashimoto, A. Yamaguchi, T. Shibata, K. Ujiie, and S. Okamoto (2007), Transition of accretionary wedge structures around the up-dip limit of the seismogenic subduction zone, *Earth Planet. Sci. Lett.*, *255*, 471–484, doi:10.1016/j.epsl.2007.01.005.

Kimura, G., E. Screaton, and D. Curewitz, and the Expedition 316 Scientists (2008), NanTroSEIZE Stage 1A: NanTroSEIZE shallow megasplay and frontal thrust, *Integr. Ocean Drill. Program Prelim. Rep.*, *316*, doi:10.2204/iodp.pr.316.2008.

Kington, J. B., and H. Tobin (2009), Implications of faulting styles in the outer wedge of the Nankai accretionary prism, Japan, *Eos Trans. AGU*, *90*(52), Fall Meet. Suppl., Abstract T21C-1827.

Kinoshita, M., H. Tobin, J. Ashi, G. Kimura, S. Lallement, E. J. Screaton, D. Curewitz, H. Masago, and K. T. Moe, and the Expedition 314/315/316 Scientists (2009), *NanTroSEIZE Stage 1: Investigations of Seismogenesis, Nankai Trough, Japan*, *Proc. Integr. Ocean Drill. Program*, 314/315/316, doi:10.2204/iodp.proc.314315316.2009.

Kodaira, S., T. Hori, A. Ito, S. Miura, G. Fujie, J.-O. Park, T. Baba, H. Sakaguchi, and Y. Kaneda (2006), A cause of rupture segmentation and synchronization in the Nankai trough revealed by seismic imaging and numerical simulation, *J. Geophys. Res.*, *111*, B09301, doi:10.1029/2005JB004030.

Martin, K. M., S. P. S. Gulick, N. L. B. Bangs, G. F. Moore, J. Ashi, J. O. Park, S. Kuramoto, and A. Taira (2010), Possible strain partitioning structure between the Kumano fore-arc basin and the slope of the Nankai Trough accretionary prism, *Geochem. Geophys. Geosyst.*, *11*, Q0AD02, doi:10.1029/2009GC002668.

Matsumoto, T., and D. R. Tappin (2003), Possible coseismic large-scale landslide off the northern coast of Papua New Guinea in July 1998: Geophysical and geological results from SOS cruises, *Pure Appl. Geophys.*, *160*, 1923–1943, doi:10.1007/s00024-003-2414-0.

Miyazaki, S., and K. Heki (2001), Crustal velocity field of southwest Japan: Subduction and arc-arc collision, *J. Geophys. Res.*, *106*, 4305–4326, doi:10.1029/2000JB900312.

Moore, G. F., T. H. Shipley, P. L. Stoffa, D. E. Karig, A. Taira, S. Kuramoto, H. Tokuyama, and K. Suyehiro (1990), Structure of the Nankai Trough accretionary zone from multichannel seismic reflection data, *J. Geophys. Res.*, *95*, 8753–8765, doi:10.1029/JB095iB06p08753.

Moore, G. F., et al. (2001), New insights into deformation and fluid flow processes in the Nankai Trough accretionary prism: Results of Ocean Drilling Program Leg 190, *Geochem. Geophys. Geosyst.*, *2*, 1058, doi:10.1029/2001GC000166.

Moore, G. F., N. L. Bangs, A. Taira, S. Kuramoto, E. Pangborn, and H. Tobin (2007), Three-dimensional splay fault geometry and implications for tsunami generation, *Science*, *318*, 1128–1131, doi:10.1126/science.1147195.

Moore, G. F., et al. (2009), Structural and seismic stratigraphic framework of the NanTroSEIZE State 1 transect, in *NanTroSEIZE Stage 1: Investigations of Seismogenesis, Nankai Trough, Japan*, *Proc. Integr. Ocean Drill. Program*, 314/315/316, doi:10.2204/iodp.proc.314315316.102.2009.

Morley, C. K. (2009), Growth of folds in a deep-water setting, *Geosphere*, *5*, 59–89, doi:10.1130/GES00186.1.

Nakanishi, A., S. Kodaira, S. Miura, A. Ito, T. Sato, J. O. Park, Y. Kido, and Y. Kaneda (2008), Detailed structural image

around splay-fault branching in the Nankai subduction seismogenic zone: Results from a high-density ocean bottom seismic survey, *J. Geophys. Res.*, *113*, B03105, doi:10.1029/2007JB004974.

Obana, K., and S. Kodaira (2009), Low-frequency tremors associated with reverse faults in a shallow accretionary prism, *Earth Planet. Sci. Lett.*, *287*, 168–174, doi:10.1016/j.epsl.2009.08.005.

Park, J. O., T. Tsuru, N. Takahashi, T. Hori, S. Kodaira, A. Nakanishi, S. Miura, and Y. Kaneda (2002a), A deep strong reflector in the Nankai accretionary wedge from multichannel seismic data: Implications for underplating and interseismic shear stress release, *J. Geophys. Res.*, *107*(B4), 2061, doi:10.1029/2001JB000262.

Park, J. O., T. Tsuru, S. Kodaira, P. R. Cummins, and Y. Kaneda (2002b), Splay fault branching along the Nankai subduction zone, *Science*, *297*, 1157–1160, doi:10.1126/science.1074111.

Park, J. O., L. Wijerathne, T. Hori, S. Kodaira, Y. Fukao, G. F. Moore, N. L. Bangs, S. Kuramoto, and A. Taira (2010), A low-velocity zone with weak reflectivity along the Nankai subduction zone, *Geology*, *38*, 283–286, doi:10.1130/G30205.1.

Plafker, G. (1972), Alaskan Earthquake of 1964 and Chilean Earthquake of 1960: Implications for Arc Tectonics, *J. Geophys. Res.*, *77*, 901–925, doi:10.1029/JB077i005p00901.

Research Group for Active Faults (1991), *Active fault in Japan, sheet maps and inventories (in Japanese with English abstract)*, 2nd ed., 437 pp., Univ. of Tokyo Press, Tokyo.

Sakaguchi, A., et al. (2011), Seismic slip propagation to the up-dip end of plate boundary subduction interface faults: Vitrinite reflectance geothermometry on IODP NanTroSEIZE cores, *Geology*, *39*, in press.

Sawyer, D. E., P. B. Flemings, B. Dugan, and T. Germaine (2009), Retrogressive failures recorded in mass transport deposits in the Ursa Basin, Northern Gulf of Mexico, *J. Geophys. Res.*, *114*, B10102, doi:10.1029/2008JB006159.

Screaton, E., et al. (2009), Interactions between deformation and fluids in the frontal thrust region of the NanTroSEIZE transect offshore the Kii Peninsula, Japan: Results from IODP Expedition 316 Sites C0006 and C0007, *Geochem. Geophys. Geosyst.*, *10*, Q0AD01, doi:10.1029/2009GC002713.

Seno, T., S. Stein, and A. E. Gripp (1993), A model for the motion of the Philippine Sea plate consistent with Nuvel-1 and geological data, *J. Geophys. Res.*, *98*, 17,941–17,948, doi:10.1029/93JB00782.

Strasser, M., et al. (2009), Origin and evolution of a splay fault in the Nankai accretionary wedge, *Nat. Geosci.*, *2*, 648–652, doi:10.1038/ngeo609.

Streiff, C, H. Tobin, and G. Moore (2009), Detailed 3-D architecture of a Thrust fault system and associated folding: Nankai Trough accretionary wedge, *Eos Trans. AGU*, *89*(53), Fall Meet. Suppl., Abstract T31A-1982.

Taira, A., et al. (1991), *Proceedings of the Ocean Drilling Program, Initial Reports*, 131, Ocean Drill. Program, College Station, Tex., doi:10.2973/odp.proc.ir.131.1991.

Takahashi, M. (2006), Tectonic development of Japanese Islands controlled by Philippine Sea plate motion (in Japanese with English abstract), *J. Geogr.*, *115*, 116–123.

Tanioka, Y., and K. Satake (2001), Detailed coseismic slip distribution of the 1944 Tonankai earthquake estimated from tsunami waveforms, *Geophys. Res. Lett.*, *28*, 1075–1078, doi:10.1029/2000GL012284.

Tobin, H. J., and M. Kinoshita (2006), NanTroSEIZE: The IDOP Nankai Trough seismogenic zone experiment, *Sci. Drill.*, *2*, 23–27, doi:10.2204/iodp.sd.2.06.2006.

Wang, K., and Y. Hu (2006), Accretionary prisms in subduction earthquake cycles: The theory of dynamic Coulomb wedge, *J. Geophys. Res.*, *111*, B06410, doi:10.1029/2005JB004094.

Zang, S. X., Q. Y. Chen, J. Y. Ning, Z. K. Shen, and Y. G. Liu (2002), Motion of the Philippine Sea plate consistent with the NUVEL-1A model, *Geophys. J. Int.*, *150*, 809–819, doi:10.1046/j.1365-246X.2002.01744.x.